Monthly Notices
of the
ROYAL ASTRONOMICAL SOCIETY

Mon. Not. R. Astron. Soc. **405,** 57–76 (2010) doi:10.1111/j.1365-2966.2010.16442.x

The host galaxies of core-collapse supernovae and gamma-ray bursts

K. M. Svensson,[1⋆] A. J. Levan,[1] N. R. Tanvir,[2] A. S. Fruchter[3] and L.-G. Strolger[4]

[1]*Department of Physics, University of Warwick, Coventry CV4 7AL*
[2]*Department of Physics and Astronomy, University of Leicester, University Road, Leicester LE1 7RH*
[3]*Space Telescope Science Institute, 3700 San Martin Drive, Baltimore, MD 21218, USA*
[4]*Department of Physics and Astronomy, Western Kentucky University, 1906 College Heights Blvd 11077, Bowling Green, KY 42101-1077, USA*

Accepted 2010 January 29. Received 2010 January 19; in original form 2009 June 11

ABSTRACT

We present a comparative study of the galactic and small-scale environments of gamma-ray bursts (GRBs) and core-collapse supernovae (CCSNe). We use a sample of 34 GRB hosts at $z < 1.2$, and a comparison sample of 58 supernova hosts located within the Great Observatories Origins Deep Survey footprint. We fit template spectra to the available photometric data, which span the range 0.45–24 μm, and extract absolute magnitudes, stellar masses and star formation rates from the resulting fits. Our results broadly corroborate previous findings, but offer significant enhancements in spectral coverage and a factor 2–3 increase in sample size. Specifically, we find that CCSNe occur frequently in massive spirals (spiral fraction ∼50 per cent). In contrast GRBs occur in small, relatively low mass galaxies with high specific and surface star formation rates, and have a spiral fraction of only ∼10 per cent. A comparison of the rest-frame absolute magnitudes of the GRB and CCSN sample is less conclusive than found in previous work, suggesting that while GRB hosts are typically both smaller and bluer than those of CCSN their total blue light luminosities are only slightly lower. We suggest this is likely due to rapid periods of intensified star formation activity, as indicated by the high specific SFRs, which both create the GRB progenitors and briefly significantly enhance the host galaxy blue luminosity. Finally, our analysis of local environments of GRBs and CCSNe shows that GRBs are highly concentrated on their host light, and further occur in regions of higher absolute surface luminosity than CCSNe.

Key words: gamma-ray burst: general – supernovae: general – galaxies: evolution – galaxies: fundamental parameters – cosmology: observations.

1 INTRODUCTION

Core-collapse supernovae (CCSNe) mark the endpoints in the lives of short-lived (lifetime $\lesssim$ few $\times 10^7$ yr), massive stars ($M \gtrsim 8\,M_\odot$). The selection of galaxies via the presence of a CCSN thus provides, in principle, an ideal mechanism for the detection of star-forming galaxies at a range of redshifts. Long-duration gamma-ray bursts (GRBs) are closely related to CCSNe, and offer similar advantages as tracers of star formation, which have been widely discussed in e.g. Jakobsson et al. (2005, 2006) and Madau, della Valle & Panagia (1998). Specifically, both CCSN and GRB production requires only a single stellar progenitor, and so they select galaxies *independently* of the galaxy luminosity. By doing so they can point at galaxies too faint to be included in flux-limited surveys, potentially providing a handle on the faint end of the galaxy luminosity function at high-z. Unlike GRBs however, CCSNe are less affected by metallicity effects, and hence they provide a more complete selection of the collapse of stars with initial main sequence masses in excess of $\sim 8\,M_\odot$. Therefore, a census of supernova host galaxies is providing a census of essentially all massive star formation at a given redshift.

One drawback in the use of supernovae (SNe) as a direct probe of star formation has been the inability to pursue searches for CCSNe beyond $z \sim 1$, due to the limitations of current technology. Out to this distance the luminosity function, and star formation rate (SFR) are reasonably well constrained through other methods. However, the installation of Wide Field Camera 3 on *Hubble Space Telescope* (*HST*), and in the longer term the launch of James Webb Space Telescope (*JWST*) offer the opportunity to push this to much higher redshift. None the less, in the interim period their potential use to 'calibrate' environmental dependencies in GRBs, and other star-forming galaxy samples, motivates their study.

A complication in the use of SNe comes from understanding biases in their observed rate introduced by dust extinction within their hosts. While the highly penetrating γ- and X-ray's from GRBs can largely circumvent problems with local extinction this is not necessarily the case for their optical afterglows. CCSNe, which are several magnitudes fainter at peak than a typical GRB optical

⋆E-mail: K.M.Svensson@warwick.ac.uk

afterglow (see e.g. Tanvir et al. 2010; fig. 9 of Bloom et al. 2009 for an extreme example), are even more prone to non-detection due to host galaxy extinction. In practise, the extent to which extinction biases the detection of either GRB optical afterglows or CCSNe remains poorly understood, although it is likely to impact both (e.g. Mannucci et al. 2003; Fruchter et al. 2006, hereafter F06; Levan et al. 2006a; Rol et al. 2007).

Effort has already been invested in studying SN hosts, and the locations of SNe within them. In particular, this has focused on large samples of SNe at low redshift, for example those found by, or overlapping with, the Sloan Digital Sky Survey (SDSS; e.g. Prieto et al. 2007) or those found in galaxies targeted by other surveys (e.g. James & Anderson 2006). These surveys offer insight into SN host properties and locations, and using local SNe, with small angular distances, allow the environments to be probed in detail. However, locally discovered SNe have historically been found by targeted searches of specific galaxy catalogues, producing a bias towards brighter host galaxies. More recent searches (e.g. SDSS and SN Factory, and in the near future Skymapper and Pan-STARRS) avoid this by repeatedly tiling blank regions of sky, although they typically find more distant SNe. Comparisons of these hosts suggest that while SNe globally trace star formation the relative fractions of Ib/c increase in highly metal enriched environments, likely reflecting the tendency for massive stars to loose their hydrogen envelopes via radiatively driven winds at higher metallicity (Prieto et al. 2007).

All CCSNe, by their nature, indicate the formation of massive stars in their hosts, while the locations of the SNe within their hosts can also be strongly diagnostic. F06 used a new pixel statistic (essentially the fraction of light contained in regions of lower surface brightness than the region containing SN or GRB) to show that GRBs are highly concentrated on the light of their hosts, and likely favour a much more massive and shorter lived progenitor than CCSNe, which trace blue light within their host galaxy. Utilizng this technique on a lower redshift sample of CCSNe found in the SDSS fields, Kelly, Kirshner & Pahre (2008) show that SNe Ic are also highly concentrated on the brightest regions of their hosts, a distribution very similar to GRBs. This may suggest that both GRBs and SNe Ic originate only from the most massive stars (Larsson et al. 2007). James & Anderson (2006) take an alternative approach of using Hα images and similarly find that SNe Ib/c are more concentrated on their hosts. They suggest that this may be due to the expulsion of SN II progenitors from their star-forming regions with moderate velocities, rather than an intrinsic tendency for SNe Ib/c to lie on brighter regions of their hosts. Should SN II typically originate from less massive stars than SNe Ib/c, then this may be expected since the transverse distances travelled over the stellar lifetime would be larger for less massive (and hence longer lived) stars.

Although there is a growing consensus that GRBs originate from different environments than the bulk of CCSNe, it is not yet clear how well the global properties of the whole host galaxy are evidence of this. Savaglio, Glazebrook & Le Borgne (2009) note that global metallicity measurements of GRB hosts are predominantly subsolar.[1] This agrees with theoretical models of GRB production, which favour lower metallicity environments (e.g. Heger et al. 2003). Furthermore, a study by Modjaz et al. (2008) suggested that SNe Ic not associated with GRBs tend to originate from more metal rich environments than SNe Ic with a GRB associated. These authors also suggested that subsolar (20–60 per cent of solar) metallicity is required to produce a GRB. A complication of testing this hypothesis is that metallicity can vary by several tenths of a dex within the hosts, both by localized enrichment (e.g. the Integral Field Unit (IFU) measurements by Christensen et al. 2008) and due to a radial gradient (e.g. Garnett et al. 1997; Rolleston et al. 2000). This makes spatially resolved spectroscopy, or direct measurements of metallicity from the afterglow spectrum valuable. However, this is impossible for a significant fraction of GRBs, since the angular distances are too small to resolve the hosts into many resolution elements. Thus, while not an ideal measure, estimates of the stellar mass or luminosity of the hosts can be used as a proxy for metallicity, and when averaged over a large number of hosts should still provide robust statements about CCSN and GRB environments.

Here we investigate the multiwavelength properties of a sample of CCSN host galaxies observed by the Great Observatories Origins Deep Survey (GOODS) and Probing Acceleration Now with Supernovae (PANS) surveys, and compare these to those of GRBs. These galaxies, lying at comparable redshift to many GRBs, although at distinctly lower-z than the mean value of $\sim$2.5 (Jakobsson et al. 2006), offer the opportunity for direct comparison of derived physical properties (e.g. mass, SFR), without the need to worry about evolutionary effects in either the galaxy luminosity function, or, in the case of GRBs, the universal evolution of metallicity. Using a large, multi-wavelength (optical through mid-IR) data set we derive physical parameters for the host galaxies of CCSNe and GRBs. This includes, rest-frame luminosities, SFRs, stellar mass and surface brightness at the GRB or SN location. Considering possible bias effects that might be present in both samples, our results broadly echo those of previous work that GRB hosts are typically smaller and less massive than those of CCSNe, most likely due to metallicity bias. GRBs also originate in brighter locations, consistent with their origin in more massive stars.

2 HOST GALAXY SAMPLES

2.1 Supernovae in GOODS and PANS

The GOODS (Giavalisco et al. 2004) survey undertook observations in two fields, centred on the Hubble Deep Field North and *Chandra* Deep Field South. These observations included deep observations with the *Hubble Space Telescope* using the Advanced Camera for Surveys (ACS) in the F450W(B), F606W(broad V/R), F814W(I) and F850LP(Z) filters. Rather than obtain the images in a single epoch the observations were made roughly every 45 d, to be sensitive to the rise time of SNe Ia at $z \sim 1$ (see e.g. Riess et al. 2004) As well as detecting a number of SNe Ia, these observations also located numerous CCSNe (e.g. Strolger et al. 2004; Dahlen, Strolger & Riess 2008; Dahlen et al. in preparation) with a mean redshift of $z \sim 0.6$ (CCSNe are generally less luminous at maximum than SNe Ia, and so visible over a smaller volume in a flux-limited sample). These SN host galaxies form an excellent sample for further study, by virtue of their selection in a blind survey, independent of galaxy luminosity (in contrast to many low-z SN searches which are targeted at specific galaxy catalogues), and because of the wide range of supporting data covering the blue optical to mid-IR regions.

These data, in addition to that secured by *HST* and described above, encompassed large programmes with *Spitzer* and also a concerted effort from ground based observatories to secure complementary near-infrared (NIR) observations and redshift catalogues. ACS images of the resulting sample of CCSN hosts are shown in Fig. 1.

[1] Although at times this conclusion depends on an assumption about the ionization parameter within the host.

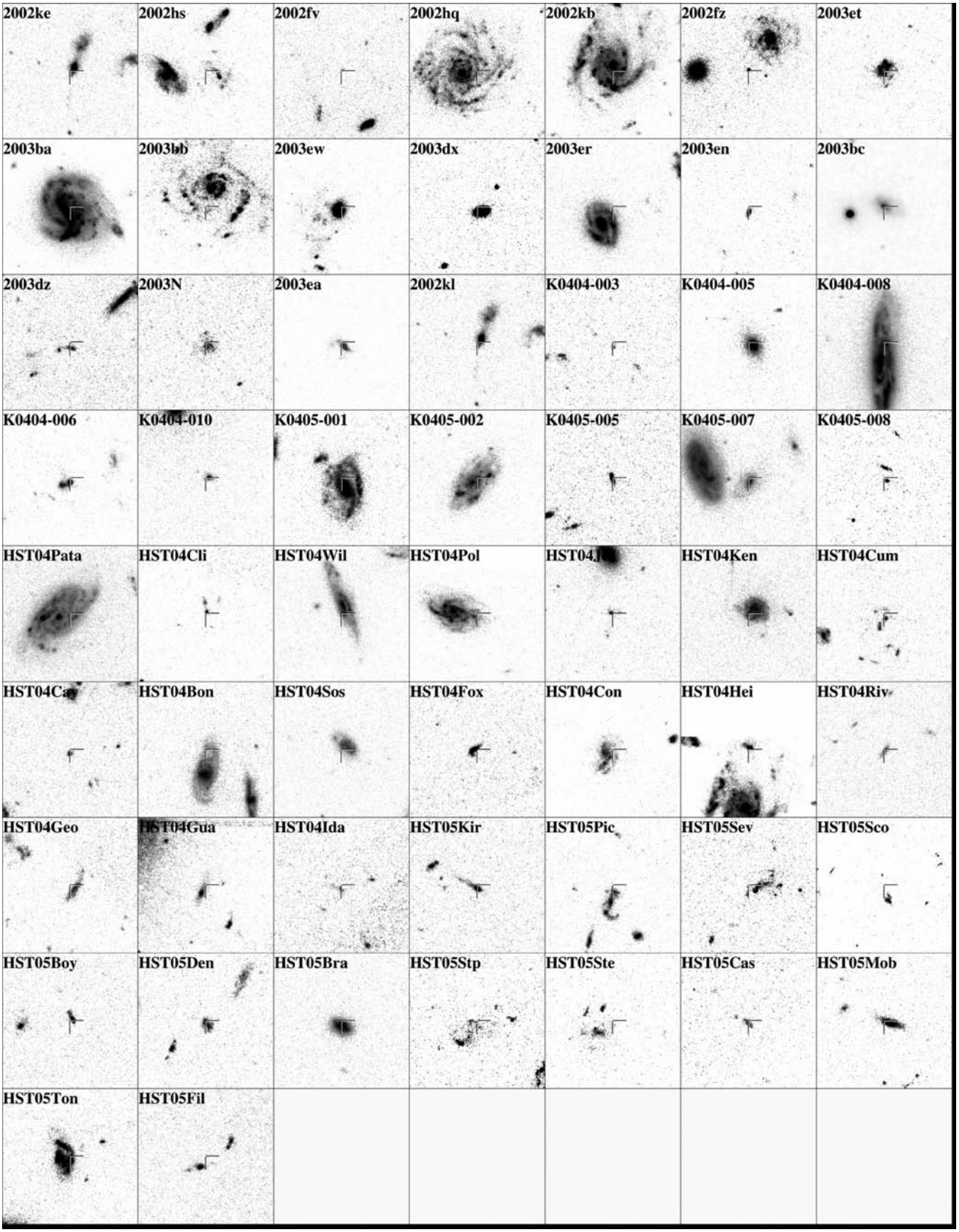

Figure 1. Mosaic image of the 58 CCSN host galaxies in the GOODS fields. These *V*-band images have a width of 7.5 arcsec and the location of the SN on the host is marked with a cross-hair.

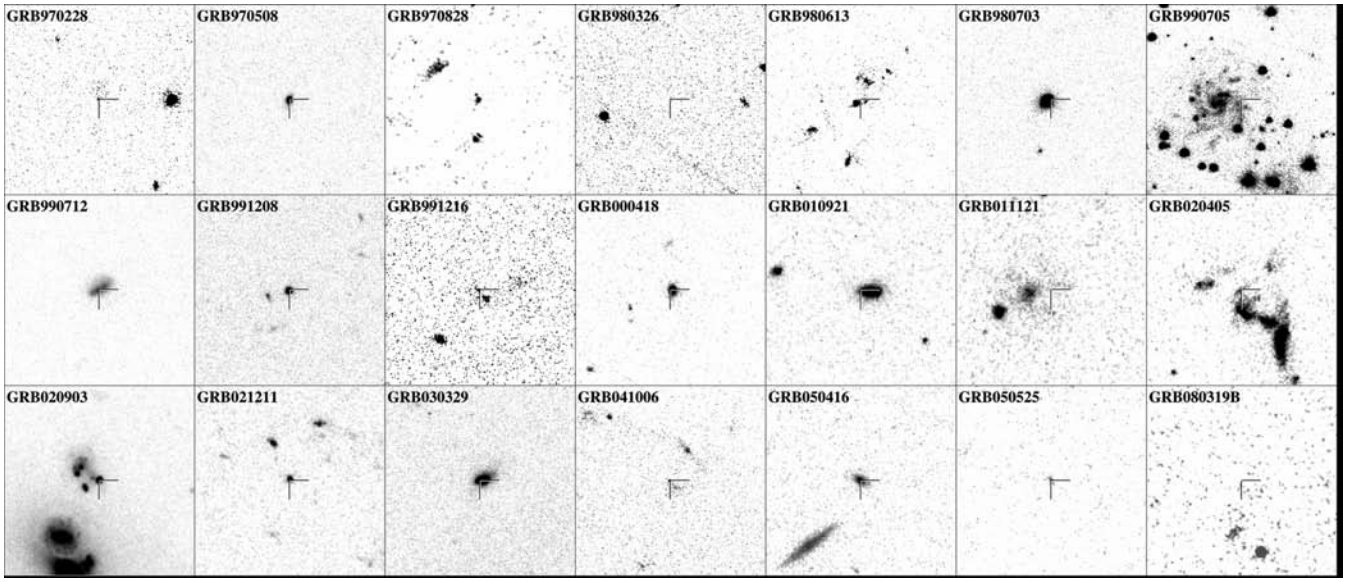

Figure 2. Mosaic image of GRB host galaxies with *HST* imaging. The images are 7.5 arcsec wide, and the locations of the GRBs on the host is marked with a cross-hair.

Each SN discovered in GOODS or subsequently PANS is typed based on the available photometric and spectroscopic data on both the SN and its host galaxy. The means of this typing is described in Strolger et al. (2004), its outcome is that the confidence in the typing of a given supernova is given by the assignation of a 'medal'. These medals, termed Gold, Silver or Bronze reflect both the quality and quantity of data available to type the SNe. The optimal diagnostic is obviously a spectrum of the SN itself, demonstrating the clear presence (or absence) of hydrogen. Spectroscopically typed SNe are given a Gold medal. In the absence of a spectrum the diagnostics used are the light-curve shape, its peak absolute magnitude, the type of host galaxy and its $U - B$ colour. Initially the light-curve shape is compared to that of an SN Ia. If this fit is poor, but the light curve well sampled then the transient is assigned as a CCSN with a Silver medal. If the light curve is inconclusive, but the host galaxy appears to be star forming then (in general) the SN is typed as CCSNe with a Bronze medal. Hence, it is possible that the inclusion of Bronze CCSNe introduces a small number of SN Ia into the CCSN sample. We discuss this issue , and other selection effects, further in Section 8. For further details on the algorithms for the classification of each SN the reader is referred to Strolger et al. (2004).

2.2 GRB host galaxies

The mean redshift of GRBs in the *Swift* era is ∼2.5 (Jakobsson et al. 2006), however a number of GRB host galaxies have been observed at redshifts across the same, or very similar range as that of the GOODS CCSN sample. To approximately match the redshift distributions we use all GRB host galaxies at $z < 1.2$. Images of the resulting sample, which have *HST* observations, are shown in Fig. 2, the subset of the hosts for which we present *Spitzer* fluxes is shown in Fig. 3. A comparison of the resulting redshift distributions is shown in Fig. 4. Using this sample enables us to create a consistent data set for CCSN and GRB hosts to perform the analysis on. This is crucial for us to be able to compare the results in a methodical way. The majority of the photometry for GRB host galaxies fitted here is taken from F06 and Savaglio et al. (2009). However, we have supplemented this data with *HST* observations of four GRB host galaxies at $z < 1.2$ (GRB/XRF 050416, GRBs 050525, 060218 and 080319B[2]) and *Spitzer* Infrared Array Camera (IRAC) observations of a further 13 hosts. The use of *HST* allows us to resolve these galaxies and thus compare not only their luminosities but physical sizes. *HST* data were reduced in the standard fashion via multidrizzle, and magnitudes and radii were determined following the method described in F06. See Section 3.1 for a description of the IRAC photometry. Although deep imaging across multiple bands is available we do not include the ambiguous GRBs 060505 and 060614, whose membership of the long-duration category of GRBs is controversial (e.g. see Fynbo et al. 2006; Gehrels et al. 2006; McBreen et al. 2008; Thöne et al. 2008, for a discussion of different viewpoints).

Although the above selection allows us to largely remove any redshift bias from the observed population, there do remain important selection differences between the GRB and CCSN host population. Whilst these are difficult to quantify they should be considered before conclusions regarding the two populations are drawn. The first effect is that the CCSNe have been located in a blind field search, and have a wide range of complementary data. This means that it is possible to derive at least a photometric redshift for every CCSN within the sample. In contrast there are a number of very faint GRB host galaxies, which do not have spectroscopic redshifts, and have insufficient bands for photometric redshifts to be plausible. Should these lie in the range of redshift we consider here ($z < 1.2$) their non-inclusion would tend to bias the observed population to higher luminosity. Indeed, even for the systems with measured redshifts, the majority of our low-z sample, ∼28 from 34 come via emission line measures in their host systems, rather than absorption lines in the afterglow, which may well create a bias towards brighter hosts, and will be considered in more detail later. In a similar spirit we have included GRBs with hosts identified both by their optical afterglows and where the X-ray afterglow is sufficient to unambiguously locate the host, however it should be noted that bursts with

[2]Host photometry extracted after subtraction of point source, see also Tanvir et al. (2010).

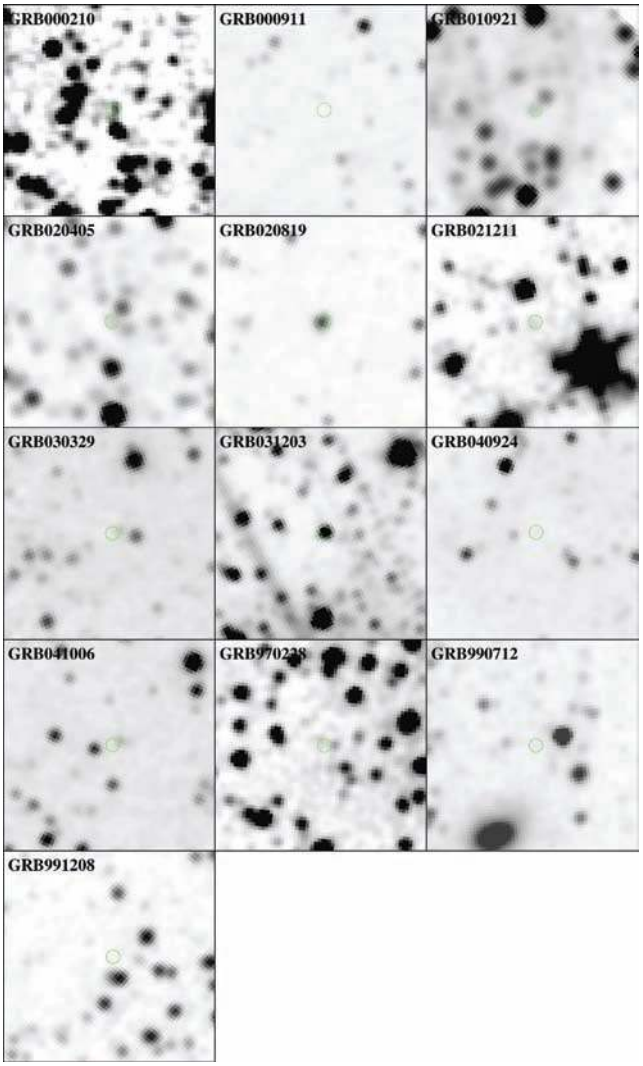

Figure 3. Mosaic image showing the GRB hosts observed with *Spitzer* IRAC. Images are in 3.6 μm where available, otherwise in 4.5 μm. The width of each tile is ∼80 arcsec.

particularly faint optical afterglows (by dust extinction) could be missed from the sample.

Finally, there are a number of host galaxies at known redshift (GRBs 980326, 990705, 991216, 050416A, 050525A, 050824 and 051016B), which have observations in a single photometric band, precluding a detailed analysis of their spectral energy distributions (SEDs). Excluding these would create a further bias within our samples, and so, rather than omitting them we derive physical parameters by assuming they can be fit with the spectral template which provides the best bit to the majority of the GRB hosts. Although this produces potential systematic errors into our analysis (e.g. the fainter galaxies may typically have different colours than the brighter systems where our templates are derived) it is preferable to their complete omission.

2.3 GOODS-MUSIC: a comparison sample

The GOODS-MUltiwavelength Southern Infrared Catalogue (MUSIC; Grazian et al. 2006) includes photometry ranging from *U* band [2.2 m European Southern Observatory telescope and Very Large Telescope (VLT)-VIsible MultiObject Spectrograph (VIMOS)] to the 8 μm IRAC band. Of the ∼14 000 objects listed in the catalogue, we select ∼6900 non-stellar, non-AGN objects with $0.1 < z < 1.2$ (redshift either spectroscopic or photometric) as a field galaxy comparison sample to the GRB and CCSN populations. The object selection for the MUSIC catalogue is made in the ACS *z*-band with a secondary selection made in the *Ks* band to obtain a higher completeness. The limiting magnitudes are reported to be $z_{\rm lim} \sim 26$ or $K_{\rm lim} \sim 24$ (AB magnitudes) at a completeness level of 90 per cent.

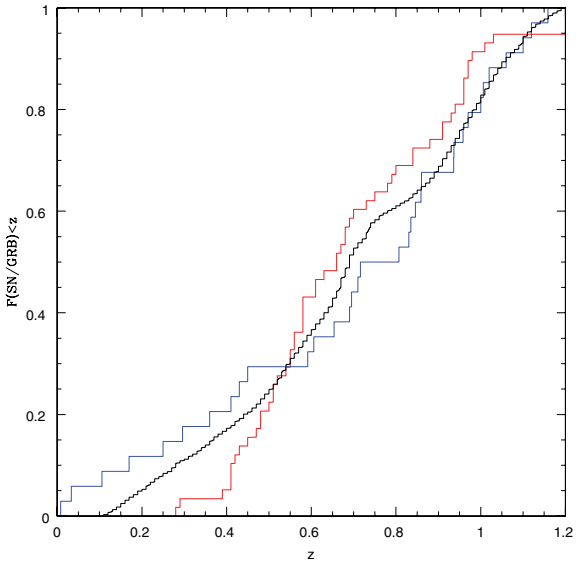

Figure 4. The redshift cumulative distributions of the GRB (blue) and SN (red) samples used in this paper. To provide similar redshift distributions we only consider GRBs with $z < 1.2$. The redshift distribution of 6900 MUSIC field galaxies is plotted in black.

Although this is a magnitude limited catalogue, whereas the GRBs and CCSNe are are detected independent of host magnitude, we consider this a good sample of field galaxies at similar redshifts to those of the GRBs and CCSNe described above. It should also be noted that method of selecting the MUSIC galaxies does not bias towards highly star-forming galaxies like the selection based on core-collapse events does. The MUSIC galaxies are hence bound to give a representation of all Hubble types, i.e. include star-forming spiral and irregular galaxies as well as passive elliptical galaxies.

3 PHOTOMETRY

Image data from GOODS is used to acquire photometry in up to 12 bands. *B, V, I* and *Z* bands are taken from *Hubble*'s Advanced Camera for Surveys (ACS). NIR *J*, *H* and *K* bands from ground based VLT using the Infrared Spectrometer And Array Camera (ISAAC). Infrared images come from *Spitzer*'s IRAC at 3.6, 4.5, 5.8 and 8 μm wavelength. Further infrared magnitudes at 24 μm (*Spitzer* Multiband Imaging Photometer for Spitzer (MIPS)) are adopted from Chary et al. (2005). The ACS data comes in high resolution (0.03 arcsec pixel^{-1}) drizzled images. We use the online cutout-service[3] to extract only the galaxy and it immediate surroundings from the larger mosaic image. The *Spitzer* images are lower resolution and one image of manageable size covers the entire field.

[3]http://archive.stsci.edu/eidol.php

Photometry on the ACS images for the 16 hosts in the original sample (F06) is initially done with the QPHOT package in IRAF. We then compared this photometry with the GOODS source catalogue (Giavalisco et al. 2004), and finding a good agreement between them, we adopted catalogue values for all of the hosts. Photometry on the ISAAC data, *J*, *H* and *K* bands was also checked for consistency between automatic source detection via SExtractor (Bertin & Arnouts 1996) and manual aperture photometry, after which we create our own source catalogue, and adopt values from this for all of the hosts. Due to the high amount of blending in the IRAC bands, automatic source detection is more challenging than for the optical and NIR bands. Photometry of the IRAC data is performed by hand, see below for a more detailed description.

In addition to photometric data we also extract measured radii from the GOODS catalogue values. These are converted into physical sizes using our assumed cosmology (Λ cold dark matter, $\Omega_{\rm M} = 0.27$, $\Omega_\Lambda = 0.73$, $H_0 = 71$ km s^{-1} Mpc^{-1}).

The majority of the host galaxy photometry for the GRB host galaxies is collected from the GHostS project, where the photometry is compiled from numerous sources, see Savaglio et al. (2009) and references within. All photometry has been corrected for Galactic extinction following Schlegel, Finkbeiner & Davis (1998).

3.1 IRAC photometry

The GOODS fields have been imaged in the *Spitzer* IRAC bands, from which we have measured and report photometry for 56 of the CCSN hosts in Table A2. A number of GRB hosts have also been imaged in the IRAC bands, in addition to the reported magnitudes collected from the GHostS project. We have analysed these images and report 26 new 3.6–8.0 μm magnitudes or magnitude limits for GRB hosts in Table A3.

Note that, due to the amount of blending between sources at IRACs resolution, for some galaxies reliable photometry could not be achieved. In these cases the catalogue entry is left blank.

The GOODS observations have been mosaiced and drizzled to a pixel scale of 0.6 arcsec pixel^{-1}, limiting magnitudes are 24–25 depending on the IRAC band and extent of the source, as estimated from *HST* imaging. The GRB observations are reduced by the standard IRAC pipeline, and have the native pixel scale of 1.2 arcsec pixel^{-1}. Limiting magnitudes are 19–23 depending on exposure times and bands of the individual observations.

The photometry is performed using the PYTHON package PYFITS provided by STScI, to extract (normal extraction) the flux inside a circular aperture with subpixel accuracy. The background is measured from blank apertures outside the host, which also provide the background standard deviation for determination of limiting magnitudes. Quoted limits are 3σ.

At the resolution of IRAC, the majority of the hosts are unresolved; in which case we use small aperture photometry and aperture corrections according to the official IRAC calibration (for the GRB hosts) or as determined from the curve of growth (CCSNe in the GOODS mosaic). If the source emission is determined to have a full width at half-maximum (FWHM) larger than the FWHM of the point spread function (PSF), we extract the photometry from a large aperture enclosing all of the flux.

4 SPECTRAL ENERGY DISTRIBUTION FITTING

The collected photometry covering wavelengths from 0.4 μm (ACS *B* band) to 24 μm (*Spitzer* MIPS) allows us to fit template SED that are close representations of the true SED within these limits. Redshifts for the CCSN hosts are determined spectroscopically in 41 cases and photometrically in 17. Spectroscopic redshifts are adopted either from Strolger et al. (2004) where available, or by querying the Team Keck Treasury Redshift Survey (TKRS; Wirth et al. 2004) for the GOODS north field, or the GOODS/FORS2 release 3 (Vanzella et al. 2005, 2006, 2008) online redshift catalogue in the south field. Our own SED fitting includes only two degrees of freedom: a wavelength independent flux proportionality, and a reddening inside the host galaxy that is wavelength dependent and calculated in the host rest frame. The reddening curve is adopted from Calzetti et al. (2000) which is derived to suit actively star-forming galaxies.

Template SEDs are collected from the literature. They include both observed SEDs of local galaxies and SEDs produced with various spectral synthesis codes. Mean templates for local ellipticals and spirals galaxies are adopted from Coleman, Wu & Weedman (1980). Synthetic GISSEL98 spectra ranging along the entire Hubble sequence are adopted from Bruzual & Charlot (1993), and synthetic fits for local galaxies ARP 220, HR 10, M51, M82, M100, NGC 6090 and 6946 are adopted GRASIL spectral libraries of Silva et al. (1998). We also include GRASIL synthetic templates fitted for sub-mm selected GRB hosts by Michałowski et al. (2008).

The best fit is given by minimizing

$$\chi^2 = \sum_{i=1}^{N_{\rm filter}} \left(\frac{f_{i,\rm obs} - b \times f_{i,\rm template} \times 10^{\frac{k(\lambda)A_v}{R_v}}}{\sigma_{i,f}} \right)^2 \quad (1)$$

with respect to the scaling parameter b, and the reddening parameter A_v. The reddening curve $k(\lambda)$ and $R_v = 4.05$ are fixed by the reddening law. The optimum SED template is transformed to its rest frame and analysed to estimate physical parameters of the host galaxy. For wavelengths between two photometric bands this means an interpolation that is more secure than a linear interpolation or assuming a globally flat SED. Some examples of our SED fits are shown in Fig. 5. Having determined the best-fitting spectral templates we derive absolute magnitudes in given photometric bands by integrating the spectrum over the response function of the filter. In Fig. 6, we plot the derived M_V values against the radii of each host galaxy.

Below we describe in brief the parameter–SED relations we use to estimate stellar mass content ($M_\star$) of the hosts, their SFRs and metallicities ($12 + \log {\rm O/H}$). Note that the SEDs are corrected for internal extinction added in the fitting procedure when estimating these properties.

5 DERIVING PHYSICAL PARAMETERS

5.1 Stellar masses

The stellar component of the total mass in a galaxy, $M_\star$, can be estimated using the rest-frame *K*-band luminosity, which samples the old stellar population with a much weaker contribution from hot and massive short lived stars. We note that some caution has been suggested when using this method on stellar populations dominated by young to intermediate aged stars, as red supergiants can become a significant source of enhanced *K*-band luminosity, and thereby lead to an overestimate of the stellar mass, e.g. Leitherer & Heckman (1995). A standard method of mass estimation is the mass to light ratio, where one assumes a proportional relationship between the stellar mass and the *K*-band luminosity. Castro Cerón et al. (2006) prescribe $M_\star/L_K \sim 0.1$ for the GRB host galaxies in their sample.

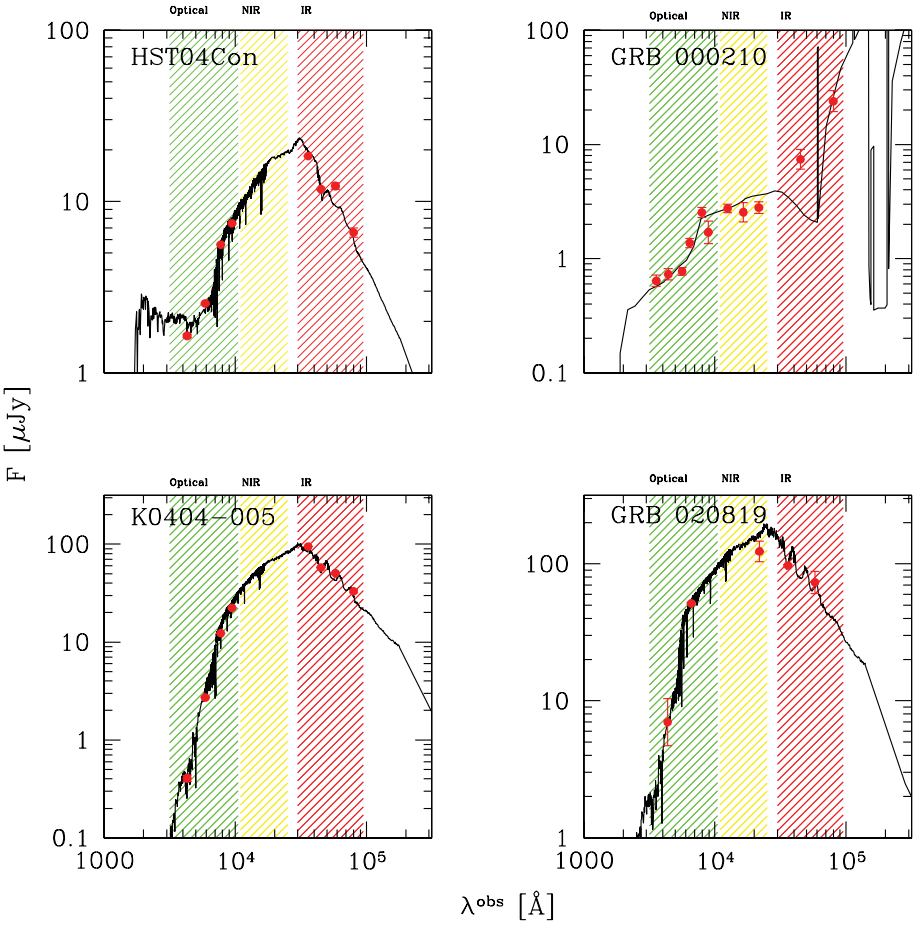

Figure 5. Example spectral energy distribution fits. Wavelengths are in the observed frame. Host galaxies of SNe HST04Con and K0404-005 have absolute V magnitudes of -21.37 and -22.53, respectively. The hosts of GRBs 000210 and 020819 have absolute magnitudes of -20.07 and -21.93, respectively

Our SED fits to these same galaxies give stellar masses in good agreement with the results of Castro Cerón et al. (2006). Here we have chosen to estimate the stellar masses with the relation of Savaglio, Glazebrook & Le Borgne (2009),

$$\log M_* = -0.467 \times M_K - 0.179, \tag{2}$$

which is calibrated on the basis of GRB hosts. [See also Glazebrook et al. (2004) for details on this mass calibration.]

5.2 Star formation rates

While the K-band luminosity is an indicator of the old stellar population in a galaxy, the U-band luminosity samples the SED contribution from the hot, massive and hence newly formed stars. Following Cram et al. (1998) we estimate the SFR by

$$\mathrm{SFR}_U(\mathrm{all}) = \frac{8.8 \times L_U}{1.5 \times 10^{22} Whz^{-1}} \mathrm{M}_\odot\ \mathrm{yr}^{-1}, \tag{3}$$

where we introduced a factor 8.8 to correct from $\mathrm{SFR}_U(\mathrm{M/M}_\odot > 5)$ to account for all star formation. It should be noted that this SFR is not model independent, but rather it assumes a certain initial mass function (IMF). Cram et al. (1998) assume a Salpeter IMF. Both stellar masses and SFRs may be inaccurately estimated if the IMF is strongly deviating from that of Salpeter. Although is more likely to agree well with CCSN-like hosts that commonly are spiral galaxies, a low mass, metal poor galaxy, initially expected to be a GRB host, could have a more pronounced top heavy IMF.

Further useful quantities are the specific SFR (SSFR) Φ:

$$\Phi = \frac{\mathrm{SFR}}{M_\star} \tag{4}$$

and the star formation surface density Σ:

$$\Sigma = \frac{\mathrm{SFR}}{\pi r_{80}^2}, \tag{5}$$

star formation per unit stellar mass and unit area in the galaxy, respectively. Since these indicate how intense the star formation is, they are in some regards a more interesting parameters to study than the SFR itself. GRB hosts are believed to have high SSFR in general, as the presence of GRB itself is evidence of the formation of massive stars. Indeed this is supported by Castro Cerón et al. (2006) who place the SSFRs of four $z \sim 1$ GRB hosts amongst the highest observed. In Fig. 7, we plot the SSFRs versus the masses for the GRB and CCSN hosting galaxy populations, as well as a selection of other high-z galaxy populations. In addition to the SSFR, we also define the surface SFR, Σ, as the SFR per unit area of the galaxy.

5.3 Metallicities

The role of progenitor metallicity in determining the outcome of massive-star core collapse has been discussed by various authors.

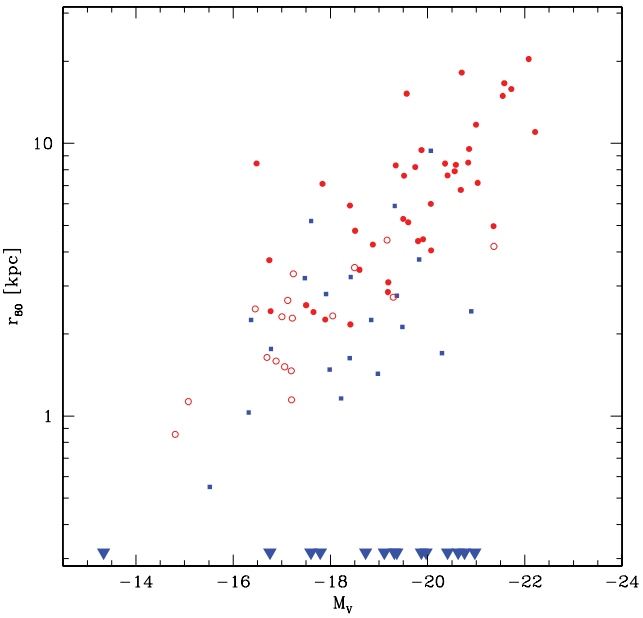

Figure 6. 80 per cent light radius versus absolute *V* band magnitude for GRB hosts (blue squares), CCSN hosts (red points, filled for hosts with spectroscopic redshifts). Blue triangles on the bottom axis are the absolute magnitudes for GRB without a measured radius (i.e. those without *HST* imaging).

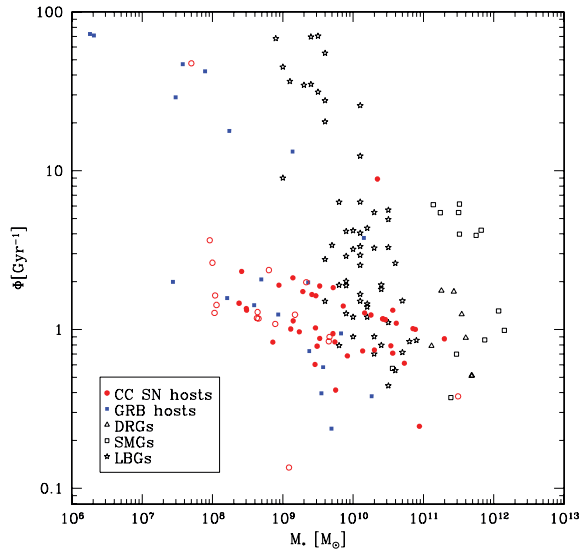

Figure 7. SSFRs versus stellar mass for GRB hosts (blue squares), CCSN hosts (red circles, filled for hosts with spectroscopic redshifts) and a selection of distant red galaxies (DRGs), sub-mm galaxies (SMGs) and Lyman-break galaxies (LBGs) compiled by Castro Cerón et al. (2006).

With the difficulties in making direct measurements of the metallicity at high redshift, mass or luminosity are commonly used as proxies. The existence of a relationship between galactic stellar mass and its metallicity has been known since Lequeux et al. (1979) published their results based on a sample of eight local galaxies. Their conclusion that low stellar mass galaxies also have lower metallicities, has since been confirmed and extended by using the much larger samples of local galaxies allowed by the SDSS, e.g. Tremonti et al. (2004). The origin of the mass–metallicity (*M–Z*) relation is still under investigation. Loss of metal enriched gas via galactic winds, accretion of low metallicity gas from the IGM, or lower star formation efficiencies in low mass galaxies could all effect the metallicity, and have been suggested as possible explanations, see e.g. Larson (1974) and Pei & Fall (1995).

Savaglio et al. (2005) calibrate the following *M–Z* relationship using 69 Gemini Deep Survey and Canada–France Redshift Survey galaxies with redshifts between 0.4 and 1:

$$12 + \log(\mathrm{O/H}) = 0.478 \log M_\star + 4.062. \quad (6)$$

This *M–Z* relation is claimed to be an improvement from the use of luminosity–metallicity relations (∼0.2 dex scatter), largely due to the small variations through the galaxies evolution in the *K*-band luminosity used to estimate the stellar mass in the galaxies. While short starburst and star formation history modify the *B*- and *V*-band luminosity greatly, the *K* band remains relatively constant.

6 LOCATIONS

In addition to their galactic environments the local scale environments of GRBs and SNe can also provide strong constraints on progenitors. If spatially resolved spectroscopy is available then the chemical evolution of the progenitor region can be probed directly, however, this is only possible in a handful of cases (e.g. Christensen et al. 2008). In the absence of detailed spectroscopy the luminosities of the region containing the transient can also be diagnostic (e.g. Östlin et al. 2008). These luminosities can be investigated both in relation to the overall host galaxy, and in absolute terms. F06 developed a pixel statistic, where the galaxy is defined by adjoining pixels above some signal-to-noise ratio limit. These pixels are then sorted into ascending order, and the pixel containing the GRB or SN is located in this ranked list. It is then possible to record a simple statistic – the fraction of host light in pixels of equal or lower surface brightness than the pixel containing the GRB or SN. This technique has the significant advantage that it provides information on the location of a given transient which is broadly independent of the morphology of the galaxy. This is particularly important for high redshift hosts, which often show disturbed and irregular morphologies. The analysis of F06 showed that GRBs are significantly more concentrated on their host light than the SN, and this is naturally interpreted as GRBs originating from more massive stellar progenitors (Larsson et al. 2007). A similar result was obtained by Kelly, Kirshner & Pahre (2008) for SN Ic, also suggesting a higher mass origin for these systems (Raskin et al. 2008).

We have extended the analysis of F06 to include more recent CCSNe and GRBs. The GRB sample is only moderately enhanced from the sample of F06, since the number of bursts with accurate positions and *HST* observations is not dramatically larger in the *Swift* era. However, the CCSN sample has increased by a factor of 4. To derive locations for the transients we co-align images taken at different epochs, one in which the SN/GRB is bright, and the other where it absent (for GRBs this is normally a very late time image, while for SN it is frequently a pre-explosion image). We then perform a direct subtraction of the two *HST* images and centroid on the variable source. We then create a galaxy mask via SExtractor and locate the pixel containing the GRB/SN in its cumulative distribution.

An alternative approach is to investigate the surface brightness of these pixels, and thus of the region of the host galaxy containing the GRB or SN. By doing this, one can make a direct comparison of the local luminosities of GRB and CCSN, essentially measuring the luminosity of the populations which host them. Since the luminosity

of a given star is roughly proportional to the cube of its mass $L_B \propto m_{\rm star}^3$, the mass (and hence age) of the stellar population dominates this statistic, more strongly than, for example, stellar number counts, where $L_B \propto N_{\rm stars}$. Since the GRB and CCSN host galaxies lie at similar redshifts the physical scales probed by this are comparable.[4]

We perform this analysis using the full sample of 58 CCSNe shown in Table 1. For the GRBs, we utilise a subset of the sample as F06, where the burst lies at $z < 1.2$ with a positional accuracy of $\lesssim$0.08 arcsec, such that the location of the burst was known to better than the *HST* (Wide Field Planetary Camera 2 or ACS) PSF, and thus the images did not require additional smoothing to emulate the observation of the host at the resolution of the error region. We have calculated the true surface brightness of the pixel that contained the CCSN or GRB event in units of $\rm L_\odot$ $\rm kpc^{-2}$ for a subsample of hosts. To account for the differing redshifts of our sample we make *K*-corrections to these values assuming that the locations of the transient have the same colours indicated by global photometry of the host galaxy. This introduces a degree of error since the colour mapping across the galaxy is unlikely to be constant. However, the signal-to-noise ratio of individual pixels is normally too low to place strong constraints on the pixel colours. We note that the application (or not) of this correction does not significantly impact our results. Our resulting distribution in shown in Fig. 10, and confirms that not only do GRBs trace a high power of light within their host galaxies, but also that GRB hosting regions are much brighter than those which host a CCSN.

7 RESULTS

The results of our analysis for CCSN and GRB hosts are shown in Tables 1 and 2, where we have tabulated the parameters derived from the fits (absolute magnitudes, SFRs, stellar masses and metallicities) along with directly measured parameters (r_{80}). The raw photometry used for the fits to the CCSN hosts is presented in Appendix A. The median *V* band absolute magnitudes are -20 (CCSN) and -19.4 (GRB), respectively, median masses are $3 \times 10^9\,\rm M_\odot$ (CCSN) and $1.3 \times 10^9\,\rm M_\odot$ (GRB), median SFRs and SSFRs are $3.6\,\rm M_\odot\,yr^{-1}$ (CCSN), $1.6\,\rm M_\odot\,yr^{-1}$ (GRB) and $1.2\,\rm Gyr^{-1}$ (CCSN), $1.2\,\rm Gyr^{-1}$ (GRB).

We perform KS tests on the cumulative distributions of all the parameters to formalise the probabilities that they are drawn from a single population. The KS probabilities are listed in Table 3, and a selection of the cumulative distribution functions are plotted in Figs 8–10.

We also compare the GRB/CCSN selected galaxies with the GOODS-MUSIC field galaxy sample. Since this sample is selected differently from the CCSN or GRB hosts, we cannot simply compare the field CDFs to the CCSN/GRB CDFs. Instead, for $M_\star$ we accumulate the mass in every step so that the step height is proportional to the mass of each field galaxy instead of constant. Hence, where the CDF for the CCSN/GRB hosts shows the number of galaxies with mass $< M_\star$ the accumulated function shows the *fraction of total mass in the field* that is accounted for by galaxies with mass $< M_\star$. The principle for the SFR and Φ is the same, but Φ weighted by SFR instead of Φ itself, i.e. this distribution function shows what fraction of star formation occurs in galaxies less active than Φ. In plotting the field galaxies in this way we would expect agreement between the field galaxy and GRB/SN curves if the probability of a GRB occurring in a given galaxy were directly proportional to the SFR (or mass) of the galaxy.

Unlike previous work we do not find any statistically significant differences between the absolute magnitudes of the GRB and CCSN host populations: the hypothesis that they are drawn from the same population is accepted with probability $P_{\rm KS} = 0.4$ for both M_B and M_V, although the median M_V of the CCSN hosts is a factor of 2 brighter in luminosity than that of the GRB hosts. Also the rest frame $B - V$ colours of CCSN hosts are also similar to those of GRBs with a probability $P_{\rm KS} = 0.2$.

However, though the stellar masses and SFRs are also broadly comparable ($P_{\rm KS} = 0.12$ and 0.15), when weighting the star formation by the galactic mass this suggest that the SSFRs for GRB hosts are higher than for CCSN ($P_{\rm KS} = 0.04$).

A comparison of the radii of the two galaxy samples also suggests, at a high significance, that GRB hosts are smaller than those of CCSN ($P_{\rm KS} = 0.003$). These results suggest that GRB hosts are on average smaller, and and more actively star forming than the CCSN counterparts. We also note the distribution of CCSN surface luminosities (Σ), which essentially combines their size and luminosity, is higher than that of GRB hosts, although not at a statistically significant level, $P_{\rm KS} = 0.14$.

Further evidence for the difference between the progenitors of CCSNe and GRBs comes from their locations. Despite a relatively small sample of GRBs with highly accurate positions on their hosts it is clear that they typically occur in regions of much higher surface brightness than CCSN, with the median difference between GRB and CCSN hosting sites being a factor of 4 in surface brightness ($P_{\rm KS} = 0.01$), and $P_{\rm KS} = 5 \times 10^{-3}$ when comparing the relative brightness ($F_{\rm light}$) of the explosion site.

8 SELECTION EFFECTS

It is clear from the above results that there are differences between the two samples in several comparative properties (e.g. r_{80}, surface brightness), while others (e.g. absolute magnitudes) appear broadly similar. A key question is therefore what selection effects could plausibly operate within the sample, and how these might impact our comparisons, could they force the two disparate distributions to look rather similar? Or alternatively, might they create apparent differences in similar underlying distributions? Below, we describe our motivation for our sample definition, and consider several selection effects, and their impact on the observed distributions of different parameters.

In the selection of our sample we have attempted to be as inclusive as possible, that is, including essentially all of the GRB hosts with $z < 1.2$ (and any available photometry) and all of the candidate CCSN hosts found within the GOODS fields. It is however necessary to explore how a number of selection effects could impact the bias of the samples, and how these would be affected if further (more restrictive) criteria were imposed. Below we discuss the effects of redshift, SNe type and extinction on the samples.

8.1 Dust obscuration

The perhaps most serious bias affecting GRB/CCSN selected galaxies is that incurred by dust obscuration along the line of sight. The brightest GRB optical afterglow observed is roughly 20 magnitudes brighter than a typical CCSN (Bloom et al. 2009; Racusin et al. 2008), and GRB afterglows typically remain brighter than their associated SNe for several days. Although a deeply buried burst could be expected to suffer from large extinctions and

[4] A pixel is roughly 150–200 pc on a side.

Table 1. Name of the associated core-collapse event, the redshift and quantities derived from the spectral energy distribution fits. Absolute magnitude in the V and B bands, SFR and stellar mass content. Hosts with only photometric redshift determination are marked in italic. Note that $F_{\rm light}$ and surface luminosity for bursts 2002fz to 2003N are calculated in the F606W filter, while the rest are in the F850LP filter.

SN name	z	r^{80} (kpc)	M_V AB mag	M_B AB mag	SFR ($M_\odot$ yr^{-1})	log $M_\star$ ($M_\odot$)	12+ log(O/H)	Surface Lum [log ($L_\odot$ kpc^{-2})]	$F_{\rm light}$
2002fv	0.7	0.86	−15.9	−15.47	0.18	8.04	7.9	7.83	0.46
2002fz	0.84	11.7	−22.08	−21.64	45.01	10.61	9.14	8.2	0.59
2002hs	0.39	8.43	−17.24	−16.89	1.3	9.11	8.42	7.67	0.09
2002hq	0.67	16.6	−22.66	−22.22	76.78	10.88	9.26	8.16	0.37
2002kb	0.58	15.82	−22.4	−22.21	30.64	10.42	9.04	8.7	0.84
2002ke	0.58	18.17	−21.61	−21.27	22.1	10.25	8.96	7.67	0.44
2002kl	0.41	5.91	−19.07	−18.9	0.6	8.86	8.3	7.35	0.14
2003ba	0.29	8.18	−20.93	−20.42	18.5	10.16	8.92	8.48	0.82
2003bb	0.96	20.37	−23.3	−22.77	173.35	11.3	9.46	7.97	0.18
2003bc	0.51	4.45	−20.65	−20.43	6.27	9.52	8.61	7.85	0.2
2003dx	0.51	2.17	−19.19	−18.94	1.59	9.15	8.43	8.34	0.45
2003dz	0.48	2.47	−16.88	−16.73	0.53	8.65	8.2	7.64	0.61
2003ea	0.98	4.38	−20.36	−20.21	4.81	9.47	8.59	8.74	0.57
2003en	0.54	1.64	−17.39	−17.19	0.14	8.03	7.9	8.61	0.91
2003er	0.63	7.16	−22.11	−21.68	32.74	10.73	9.19	8.02	0.08
2003et	1.3	4.97	−21.63	−21.51	48.3	10.56	9.11	8.62	0.86
2003ew	0.58	15.21	−20.58	−20.18	10.15	9.86	8.77	8.48	0.71
2003N	0.43	3.73	−17.51	−17.15	1.66	9.23	8.48	7.89	0.69
K0404-005	0.79	8.34	−22.29	−21.66	21.52	10.94	9.29	8.81	0.61
K0404-003	0.55	1.13	−15.54	−15.37	0.16	8.06	7.91	7.65	0.56
K0404-006	0.41	2.4	−18.31	−18.02	2.94	9.52	8.61	8.48	0.79
K0404-008	0.28	9.45	−21.16	−20.59	27.12	10.54	9.1	9.0	0.7
K0404-010	0.61	2.31	−18.83	−18.08	0.17	9.09	8.41	8.4	0.59
K0405-001	1.01	11.0	−22.7	−22.48	196.31	10.35	9.01	8.19	0.28
K0405-002	0.56	8.43	−21.18	−20.9	5.63	9.92	8.8	8.46	0.8
K0405-005	0.68	2.55	−18.17	−18.05	0.4	8.48	8.12	7.93	0.3
K0405-007	0.5	4.78	−19.73	−19.28	1.72	9.46	8.58	9.32	0.98
K0405-008	0.88	3.32	−18.21	−17.72	1.85	9.17	8.45	8.03	0.6
HST04Pata	0.41	9.53	−21.87	−21.47	33.12	10.46	9.06	8.6	0.53
HST04Cli	0.75	1.52	−17.45	−17.33	0.85	8.89	8.31	8.23	0.72
HST04Wil	0.42	8.3	−20.2	−19.9	2.41	9.49	8.6	8.27	0.69
HST04Pol	0.56	7.9	−21.47	−21.14	14.89	10.3	8.99	7.87	0.14
HST04Jef	0.96	2.26	−18.37	−18.31	0.41	8.48	8.12	8.12	0.69
HST04Ken	0.52	5.28	−20.53	−20.13	2.34	9.75	8.72	8.38	0.7
HST04Cum	0.97	3.44	−18.78	−18.72	2.93	9.14	8.43	8.3	0.69
HST04Cay	0.8	1.15	−17.61	−17.41	1.5	8.8	8.27	7.9	0.2
HST04Bon	0.66	8.49	−22.15	−21.57	71.59	10.85	9.25	8.09	0.19
HST04Sos	0.55	4.41	−20.13	−19.83	4.13	9.66	8.68	8.46	0.8
HST04Fox	0.69	2.33	−18.59	−18.49	0.56	8.64	8.19	8.07	0.35
HST04Con	0.84	7.62	−21.27	−20.97	9.99	10.13	8.91	8.23	0.5
HST04Hei	0.58	14.92	−22.29	−22.06	31.05	10.43	9.05	7.4	0.14
HST04Riv	0.61	2.42	−17.43	−17.27	0.35	8.38	8.07	7.99	0.58
HST04Geo	0.94	5.13	−20.09	−19.97	3.34	9.28	8.5	8.62	0.85
HST04Gua	1.26	4.19	−22.9	−22.06	117.58	11.49	9.55	8.48	0.43
HST04Ida	0.91	1.59	−17.14	−17.1	0.51	8.63	8.19	8.38	0.77
HST05Kirk	0.45	2.65	−17.49	−17.36	2.37	7.7	7.74	8.13	0.74
HST05Pic	0.91	6.0	−20.49	−20.42	4.31	9.41	8.56	8.3	0.62
HST05Sev	0.96	7.61	−19.87	−19.87	1.67	8.94	8.34	7.6	0.07
HST05Sco	0.93	3.5	−18.96	−18.79	3.79	9.65	8.68	7.56	0.0
HST05Boy	0.66	2.28	−17.45	−17.47	0.26	8.0	7.89	8.24	0.69
HST05Den	0.97	3.09	−19.82	−19.67	2.97	9.46	8.59	8.53	0.87
HST05Bra	0.48	2.85	−20.18	−19.8	4.59	9.74	8.72	9.01	0.94
HST05Str	1.03	4.05	−20.56	−20.37	9.52	9.72	8.71	7.31	0.0
HST05Cas	0.73	1.47	−17.68	−17.61	0.33	7.96	7.87	8.09	0.77
HST05Mob	0.68	4.25	−19.79	−19.47	4.86	9.71	8.7	8.1	0.32
HST05Ton	0.78	6.75	−21.73	−21.31	25.92	10.56	9.11	8.6	0.76
HST05Fil	1.21	2.73	−19.37	−19.38	4.28	9.33	8.52	7.66	0.0
HST05Ste	0.47	7.1	−18.37	−18.27	0.6	8.41	8.08	7.7	0.88

Table 2. As Table 1 but for GRB host galaxies. Surface luminosity and $F_{\rm light}$ depend on accurate positional information, hence, they are only calculated for hosts with *HST* imaging and positional errors <0.1 and <0.15 arcsec, respectively.

GRB name	z	r^{80} (kpc)	M_V AB mag	M_B AB mag	SFR ($M_\odot$ yr^{-1})	log $M_\star$ ($M_\odot$)	12 + log(O/H)	Surface lum. ($L_\odot$ kpc^{-2})	$F_{\rm light}$
GRB 970228	0.695	3.2	−18.13	−18.04	0.25	8.21	7.99		
GRB 970508	0.835	1.48	−18.37	−18.22	3.08	8.24	8.0	8.48	1.0
GRB 970828	0.958	2.8	−19.43	−18.8	2.17	9.57	8.64		
GRB 980326	1.0		−12.81	−13.24	0.01	4.71	6.31		1.0
GRB 980425	0.0085		−18.34	−18.09	0.34	8.53	8.14		
GRB 980613	1.1	3.75	−20.77	−20.42	6.34	9.83	8.76		0.42
GRB 980703	0.97	2.42	−21.49	−21.23	53.79	10.15	8.92		0.56
GRB 990705	0.86	9.38	−19.57	−19.98	3.31	7.89	7.84		
GRB 990712	0.43	2.25	−19.57	−19.43	1.07	8.94	8.33	8.39	0.97
GRB 991208	0.71	1.16	−18.8	−18.68	0.55	8.59	8.17		0.94
GRB 991216	1.02	2.25	−15.94	−16.3	0.13	6.26	7.05		
GRB 000210	0.846		−20.01	−19.85	1.89	9.21	8.47		
GRB 000418	1.12	1.7	−20.55	−20.48	18.16	9.14	8.43		0.45
GRB 000911	1.06		−19.37	−19.2	1.36	9.09	8.41		
GRB 010921	0.45	2.76	−20.17	−19.87	1.74	9.38	8.54	8.62	0.44
GRB 011121	0.36	5.89	−20.14	−19.75	1.4	9.55	8.63	8.36	0.51
GRB 020405	0.69		−21.06	−20.75	4.96	9.89	8.79	8.31	0.59
GRB 020819	0.41		−22.06	−21.53	14.5	10.52	9.09		
GRB 020903	0.25	1.43	−19.33	−19.34	1.02	8.69	8.22	8.44	0.96
GRB 021211	1.006	1.63	−19.95	−19.12	6.95	10.26	8.97	8.67	0.76
GRB 030329	0.17	1.03	−16.67	−16.52	0.87	7.47	7.63	8.16	0.99
GRB 031203	0.1055		−19.07	−18.52	0.44	9.24	8.48		
GRB 040924	0.859	3.23	−19.55	−19.1	4.54	9.36	8.54		
GRB 041006	0.716	5.19	−18.73	−18.29	1.17	9.69	8.69	8.23	
GRB 050223	0.5915		−20.77	−20.51	4.3	9.81	8.75		
GRB 050416A	0.6535	2.12	−18.96	−19.38	1.77	7.58	7.68	8.98	0.97
GRB 050525A	0.606	1.76	−16.25	−16.68	0.15	6.31	7.08	8.19	0.95
GRB 050824	0.83		−18.62	−19.02	1.37	7.45	7.62		
GRB 050826	0.296		−20.97	−20.28	1.39	9.93	8.81		
GRB 051016B	0.9364		−19.35	−19.77	2.54	7.76	7.77		
GRB 051022	0.807		−21.55	−21.23	23.85	10.49	9.07		
GRB 060218	0.0331	0.55	−15.92	−15.92	0.05	7.44	7.62		
GRB 061126	1.1588		−22.36	−21.61	51.34	11.16	9.4		
GRB 080319B	0.937		−17.49	−17.23	0.13	8.07	7.92	8.58	

non-detected or very faint optical afterglows (so-called 'dark' bursts, see e.g. Fynbo et al. 2001; Lazzati, Covino & Ghisellini 2002; Jakobsson et al. 2004; Levan et al. 2006a; Rol et al. 2007; Perley et al. 2009) dust destruction by X-rays could still be effective enough to allow UV/optical observations of the afterglow according to Fruchter, Krolik & Rhoads (2001). However, Fynbo et al. (2009) suggests very convincingly that dark bursts *may not* be representative of the general GRB population, and trace different environmental properties than bursts with detected optical afterglows. Either way, even in the absence of any transient optical emission it is possible to identify a redshift for a GRB from its X-ray identified host galaxy (e.g. GRB 970828 or 051022; Groot et al. 1998; Rol et al. 2007). This relative insensitivity to dust obscuration is one of the key advantages of GRBs over many other techniques for high redshift exploration. Indeed, while it is interesting to note that both spiral host galaxies in the GRB sample [GRB 990705 (Masetti et al. 2000) and GRB 020819 (Jakobsson et al. 2004)] are from bursts which were plausibly dust obscured, in general the GRB afterglow is much brighter than any SN, and hence if the low spiral fraction in GRBs were due to dust obscuring many optical afterglows, we would expect to see an even stronger bias against spiral galaxies in the CCSN sample, which is not the case.

Indeed, SNe are likely much more strongly affected by dust that GRBs; studies of local starburst galaxies in the IR suggest that a reasonable fraction of CCSNe may occur in deeply enshrouded regions of their hosts (Mannucci et al. 2003), essentially invisible to optical observations. This problem becomes even more extreme at moderate redshift, where optical observations probe rest-frame UV light, thus one may then suspect that the CCSN sample may be incomplete due to SNe being lost to dust extinction. Since the dustiest galaxies tend to be those which are most massive it is likely that any dust obscuration would remove the brightest hosts from our sample, and would imply that any impact on a CCSN selected galaxy population from dust, would most likely act to decrease its mass distribution.

Indeed, while MIPS observations of the GOODS fields (Chary et al. 2005) suggest that ∼60 per cent of SN hosts are detected, this is not true for GRB host observations; Le Floc'h et al. (2006) find a detection rate of only ∼20 per cent implying that dust may well have a larger impact on CCSN detection than GRBs. In contradiction to this we note that the deeper observations of the CCSN host may be a factor in the higher detection rate, and that comparing the detection rate above a uniform depth results in more similar rates.

Table 3. KS probabilities for comparison of physical properties between GRB and CCSN host galaxies. Showing the probabilities that the distributions of each parameter are drawn from the same population. The parameters compared are the global SFR, the absolute B- and V-band luminosities (M_V and M_B), the $B-V$ colour, the luminosity of the pixel underlying each GRB/SN $L_{\rm surface}$, the 80 per cent light radii r_{80}, the SSFR Φ, the surface SFR Σ and the location of the GRB/SN on their cumulative host galaxy light.

	$P_{\rm KS}$ (all)
M_V	0.41
M_B	0.39
$B-V$	0.23
SFR	0.15
Σ	0.14
$M_\star$	0.12
Φ	0.04
$L_{\rm surface}$	0.01
r_{80}	0.003
$F_{\rm light}$	5×10^{-3}

8.2 Evolution of global properties

Although both CCSNe and GRBs originate from young systems, this does not necessarily indicate that the relations between broad-band properties and underlying physical conditions should be the same for each sample. Since we explicitly assume a direct proportionality between the K band an stellar mass, or U band and SFR, any systematic differences in these proportionalities between the two sample could create a bias in the observed populations. The morphological properties of the CCSN hosts, combined with their redder colours suggest that there is a significant older population already in place. In a sense these galaxies should therefore be reasonably representative of the samples of local star-forming galaxies from which the stellar-mass and SFR indicators are derived. In contrast, GRB hosts are apparently irregular, and several studies indicate they are extremely young, with ages for the *dominant* stellar populations of under 10^7 yr (e.g. Christensen, Hjorth & Gorosabel 2004; Levesque et al. 2009) For very young systems the K-band luminosity is dominated by young stars (e.g. Berta et al. 2004), and therefore may well be enhanced per unit stellar mass, such an effect would cause us to significantly *overestimate* the GRB host galaxy masses. Secondly, in very young stellar systems ($t < 10^8$ yr) the relation between U-band luminosity and SFR is not constant, but *underestimates* the SFR for a given U-band luminosity (Verma et al. 2007). In other words, the very young stellar ages derived from detailed studies of individual GRB host systems (e.g. Levesque et al. 2009) suggest that our derived properties for the GRB hosts may be systematically too massive, with too low a SFR. Were this corrected it is likely that the GRB and CCSN sample would seem more disparate than we observe. To partly quantify this effect it is relevant to note that not only is there a relationship between K-band luminosity and stellar mass, but also between effective radius and stellar mass (Bernardi et al. 2003; Damjanov et al. 2009). Since the median sizes of the GRB and SN hosts differ by a factor of ∼2, this would also suggest that the median mass of a CCSN host would be a factor of ∼4 larger. In essence, it is not possible for both the GRB and SN hosts to satisfy both of these relations, given the very young stellar ages of GRB hosts, and their likely impact on the broad-band properties we hence suggest that it is the morphological (and size) difference which defines the GRB and SN populations, and that CCSN hosts are indeed typically more massive than those of GRBs.

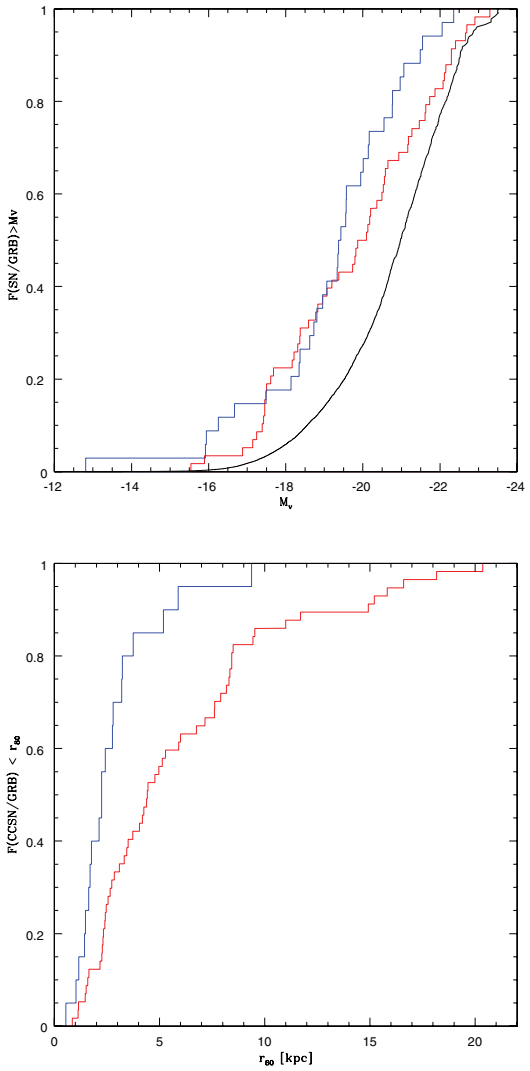

Figure 8. Cumulative distributions of the absolute V-band magnitudes of GRB hosts (blue line), CCSN hosts (red) and the MUSIC field galaxy sample (black) with absolute magnitudes accumulated by luminosity. (Upper) and 80 per cent light radius (Lower).

8.3 Redshift

A further selection effect to consider is the origin of the redshifts for any given CCSN or GRB. For CCSNe the broad-band photometric data available enable the derivation of a photometric redshift (although see below). In contrast most GRB hosts do not have this coverage and therefore redshifts come primarily from either emission redshifts of the hosts or via absorption redshifts derived via observations of their afterglows. Although emission line flux is not directly proportional to host continuum magnitude there is a broad dependence which means that emission line redshifts can normally

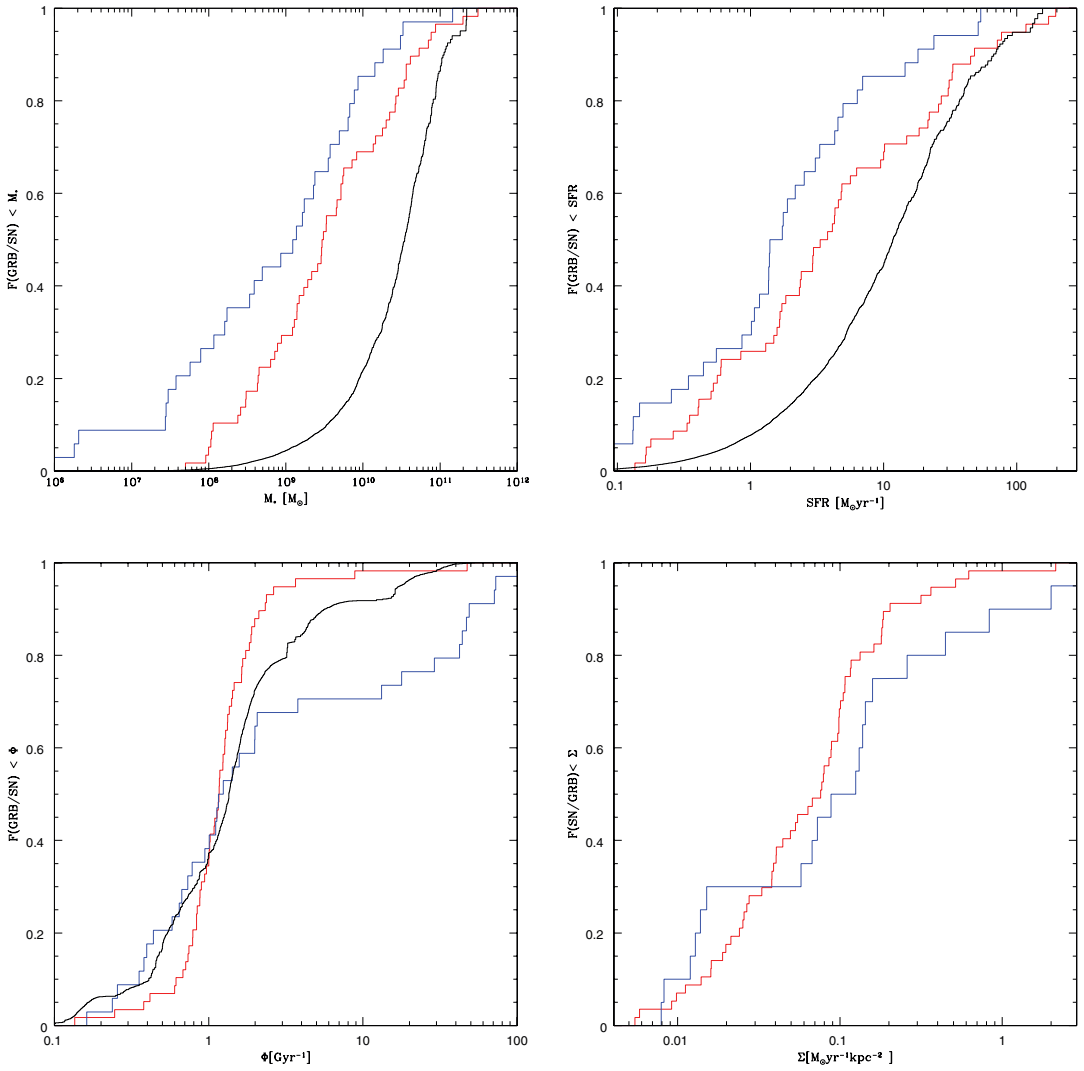

Figure 9. Top left: cumulative distribution of CCSN (red) and GRB (blue) host galaxy masses along with fractional mass distribution in field galaxies (black). Note that for CCSN and GRB we plot the fraction of number of galaxies, while for the field galaxies, we plot the fraction of mass. Top right: cumulative distribution of the SFRs. The field galaxy sample is weighted by the individual galaxies SFR. Lower left: cumulative distribution of CCSN and GRB SSFRs. The field galaxies SSFR is weighted by the SFR in each galaxy. Lower right: the surface SFRs of GRB and supernova host galaxies, assuming a uniform distribution of star formation over r_{80}.

only be derived from brighter hosts. In contrast absorption redshifts can be determined *independently* of host magnitude (e.g. Berger et al. 2002; Hjorth et al. 2003; Vreeswijk et al. 2004), although this is not necessarily straightforward for low redshift bursts where the UV metal lines are not redshifted into the optical band. The consequence of this is that the requirement of a measured redshift biases our GRB sample toward intrinsically brighter hosts. Indeed, if we perform a Kolmogorov-Smirnov (KS) test between the hosts with absorption line spectra and those with emission line redshifts we find that the sample with absorption redshifts is fainter than those with redshifts derived from emission lines; KS probability of being drawn from the same distributions is only $P_{\rm KS} = 0.001$. In other words, it is plausible (though not certain) that we are missing a population of intrinsically faint, low to moderate redshift GRB hosts.

In part because of this above discussion we have included photometric redshifts for the CCSN sample where possible. Since, if the photometry is sufficiently well sampled, they do provide a necessary handle on the faint hosts not observed with TKRS or GOODS/FORS2. Though exclusion of hosts without spectroscopic redshift, would narrow down the sources of random errors, it would also bias the sample towards observationally bright, and thus, on average towards more luminous host galaxies. We note that the mean apparent magnitudes and absolute magnitudes are 23.54 and −19.8 for the complete sample, and 22.79 and −20.5 for hosts with spectroscopic redshifts, hence we include all CCSN hosts in the sample, independently of how the redshift was determined.

8.4 SN typing

Approximately half of the CCSNe are typed with low confidence (Bronze medal), hence there is a probability that we have a fraction of SN Ia hosts in the sample. SNe Ia can appear in both old stellar population due to long delay times between star formation and explosion, as well as exploding rapidly after the formation of the progenitor system. Since they are more likely than CCSNe to occur in latent stellar populations, this could clearly affect the colours, SFRs and SSFRs of the CCSN sample we have analysed. It is,

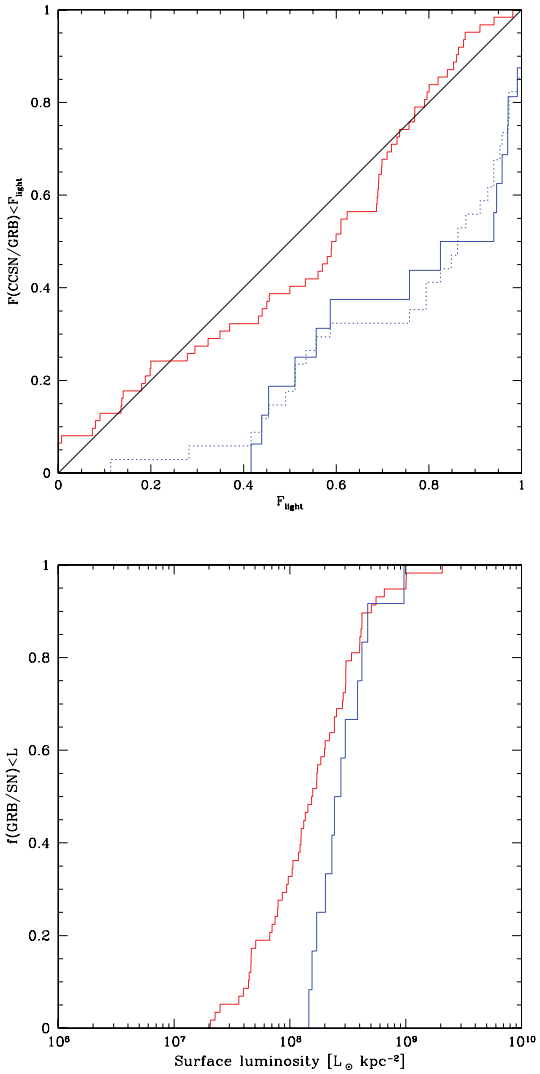

Figure 10. Local environmental properties of the GRB and CCSN sample. Upper: the locations of SNe (red) and GRBs (blue) on the light distributions of their host galaxy. The blue dashed line shows the locations for GRBs at $z < 1.2$, while the solid line all bursts in the sample of F06. Lower: the absolute surface brightness under the transient location in $L_{\odot}$ kpc^{-2}. Both in relative and absolute terms GRBs appear more concentrated on their host galaxy light.

however, more difficult to determine how the mass distribution will be affected. Performing SED-fitting and estimating the host stellar masses of the GOODS-detected SNe Ia give a ∼0.2 dex higher mass distribution, though the KS probability concludes they are consistent with a single distribution.

As a further test to rule out that the results have been disturbed by mistyped SNe, we perform the KS test also on the sample containing only securely typed CCSNe (Gold and Silver medal). We discover that the G+S sample are brighter in the *V* band absolute magnitudes, but not significantly more massive than the complete sample. Using this subsample the absolute magnitudes are dissimilar to the GRB sample at a statistically significant level ($P_{\rm KS} \sim 0.06$), and the mass distributions have almost unchanged $P_{\rm KS} = 0.13$.

However, we note that this in part may well be due to the reduced numbers of hosts in the sample (G+S:23, B:35) when culling by SN confidence level, as well as due to the fact that this sample is also brighter in apparent magnitudes. We note that, though some influence cannot be ruled out, the conclusions are overall not changed by including or excluding parts of the sample based on SN typing.

While there is no evidence that SN Ic host galaxies differ from the hosts of other types if CCSNe when considering global properties, Kelly et al. (2008) gives a strong indication that they typically lie on the brighter parts of the host. We note that such a bias introduced by SN Ic in the sample would act to decrease the separation between the CCSN and GRB populations, though this effect is most likely small and would only effect the $F_{\rm light}$ and surface luminosity distributions, implying that their intrinsic distributions are even more separate.

8.5 The overall impact of selection effects on the observed sample

Above we have considered various biases, which are likely to be operating within our sample of GRB and CCSN host galaxies. These include selection effects, which are inevitably introduced into any magnitude/flux-limited sample and also intrinsic systematic errors which propagate through our sample due to our incomplete knowledge of the detailed physical states of the galaxies we are studying. Overall, we consider the apparent differences in size and morphology to be compelling. Although dust extinction will impact both SN and GRB hosts we believe it should impact SN more, and hence the different morphologies observed are inconsistent it being a dominant selection effect. Similarly, the lack of GRB hosts with photometric redshifts biases them to the brighter hosts, where emission line redshifts can be obtained, the difference between apparent host luminosities of bursts with host emission, or afterglow absorption redshifts is indicative that there may be a faint population of GRB hosts (currently GRBs without redshift measurements) omitted from our sample. Finally, the extreme properties of the GRB stellar populations based on detailed population modelling (e.g. Levesque et al. 2008) imply that using empirically determined relationships between monochromatic luminosities and physical properties is not necessarily optimal. Hence we conclude that the environments of CCSNe and GRBs are indeed different, and consider explanations for this below.

9 DISCUSSION

Although SNe and GRBs are closely related phenomena, one question of interest is the characteristic environments – both local and galactic – in which they form. By contrasting the environments of the two transient events we can obtain clues to their stellar progenitors. This in turn provides observational constraints to the pathways which can create GRBs and is central to understanding any biases in using GRBs as cosmological probes (e.g. as probes of star formation) as opposed to galaxy samples selected in flux-limited surveys. For example, our comparison with the MUSIC sample suggests that roughly a few per cent of the star formation tracked by CCSN and GRB is too faint to be included in the flux-limited sample. Finally, the fraction of stars which may create GRBs as a function of environmental properties can feed into predictions of high redshift (and hence low metallicity) GRB rates, as an input for potential future GRB missions targeting high redshift GRBs (e.g. EXIST[5]).

The conclusion of F06 is echoed by our results, showing that GRB hosts are consistently fainter and have more irregular morphology than their SN counterparts. Given the well calibrated relation between luminosity and metallicity, e.g. Tremonti et al. (2004), this is

[5]http://exist.gsfc.nasa.gov/

most clearly explained by a preference for GRBs in low metallicity environments. F06 also compared how CCSNe and GRBs trace blue light in the hosts. The findings are consistent with the CCSN tracing the blue light, and therefore broadly the global star formation. The GRB population on the other hand appears to be significantly more concentrated on the brightest regions of the galaxies. This could naturally be interpreted as GRBs being due to the collapse of more massive stars, probably with initial masses $>20\,M_\odot$ (Larsson et al. 2007). These stars form in large OB-associations, and, since stellar luminosity traces a high power of stellar mass (crudely $L_\star \propto m_{\rm star}^3$), produce much more light than stars of lower mass, even those which produce SN.

This is further reflected in an analysis of the surface brightnesses measured *directly* under the transient position, which accepts the possibility that they are being drawn from the same population with a KS probability of only 0.01. Furthermore a comparison of locations within the hosts following the method of F06 is even more compelling suggesting that the two distributions cannot be reconciled with a probability higher than $P_{\rm KS} = 5 \times 10^{-3}$. These results are naturally explained by the origin of GRBs in very young, and subsequently very massive stellar progenitors.

The so far most successful progenitor model for long GRBs is the collapsar model (Woosley 1993), predicting that the bursts are the result of the collapse of rapidly rotating cores from massive stars. The metallicity to a large extent determines the rate of mass loss that is due to stellar wind in the progenitor star, and hence also the angular momentum loss. Core collapse progenitors arising in low metallicity environments support only weak winds and may be able to retain a large fraction of the initial rotation. As rapid rotation is thought to be one of the key the discriminators between GRB and CCSN explosions, it is natural to expect that GRB progenitors may therefore form in lower metallicity environments. However, all SNe so far associated with GRBs are of the Ic variety, suggesting that the hydrogen envelope has been lost, and indicating that simple low metallicity may not be sufficient to create GRBs and that in single stars more exotic processes such as complete mixing on the main sequence (e.g. Yoon & Langer 2005) may be necessary.

Introducing the option of a binary star evolution (e.g. Podsiadlowski et al. 2004; Levan, Davies & King 2006b; van den Heuvel & Yoon 2007) can potentially create GRBs across a wider range of metallicity. A binary scenario is suggested where two massive ($M > 8\,M_\odot$) stars after main sequence evolution and separation tightening through a common envelope phase end up as a neutron star or black hole and helium core binary. Tidal locking of the helium cores rotation enables enough angular momentum to create a torus, and the accretion of this on to the central compact object at core collapse powers the GRB. Although this scenario remains possible at all metallicities, magnetic braking by a strong stellar wind could bias also binary progenitors towards low metallicity environments.

The discrimination between the different progenitor routes can potentially be made via metallicity measurement for the host galaxies. While binary channels will operate at all metallicities (albeit with an increased rate toward the lower end) single star evolution may produce a sharp cut-off in the metallicity at which GRBs can be created. The two possibilities can potentially be tested via metallicities for a large sample of GRB hosts.

The task of host galaxy metallicity measurement is made difficult owing to the large redshift of many bursts. Therefore, many studies of long burst host galaxy metallicities have used a luminosity–metallicity relation for the estimate. Other possibilities to measure the local metallicity are by using the GRBs optical or X-ray afterglow as a probe, and study the absorption lines when it shines through the immediate environment (see e.g. Vreeswijk et al. 2004; Chen et al. 2005; Starling et al. 2005).

Wolf & Podsiadlowski (2007) studied the host metallicities using largely the same sample as F06, but with a more conservative redshift constraint. Their modelling of metallicity dependent efficiency for producing GRBs suggests that progenitor metallicity is of importance, their favoured model being one with constant efficiency up to nearly solar composition and with a sharp cut-off, although they make the implicit assumption that the shape of the mass metallicity relation for GRB hosts is the same as for field galaxies. While this may be the case, it is far from clear (Modjaz et al. 2008). The authors also comment on the global versus local metallicity *within* the galaxy. Importantly, without spatially resolved spectroscopy, the variations between metallicity in different parts of the galaxy can be almost as large as the scatter in the *M–Z* relationship. Thus spectroscopy without spatial resolution may not yield better results (for the progenitors metallicity) than using mass or *K*-band luminosity as proxy.

Our new sample of GRB and CCSN hosts is a factor of 2–4 larger than previously available samples, and with the broad-band coverage allows us to derive physical parameters. It is interesting to investigate how our results may be interpreted in terms of the above discussion.

In contrast to previous studies, we do not find highly significant (considering the *KS* test) differences between the M_V or M_B distributions for GRB and CCSN hosts, although the median GRB hosts is roughly a factor of 2 fainter than the median of CCSNe (see Fig. 9 where we plot the cumulative distribution function of M_V). Considered alone, this is inconsistent with previous studies, although it should be noted that the distinction in absolute magnitude is previous samples was the least significant of a number of parameters compared. The origin of the apparent discrepancy between our results and those of F06 is down to the combination of two factors. First, we attempt to derive absolute magnitudes based on spectral templates, rather than assuming flat spectrum sources. Secondly, our larger sample of CCSNe is apparently fainter than the sample considered in F06. Indeed, the mean apparent magnitude of the new CCSN sample is $\sim$1 magnitude fainter, despite a similar redshift distribution. Although the new larger sample of CCSNe does not suggest an overall globally different luminosity function it is particularly interesting to note that the sample of GRB hosts contain no galaxies brighter than $M_V \sim -22.4$, while the CCSN host population continues to $M_V \sim -23.3$. Given the luminosity–metallicity relations discussed above this may well be consistent with a sharp cut-off in the metallicity at which a GRB can be created. Comparison of these two distributions with models for GRB efficiency in binary and single star models as a function of metallicity may help to elucidate this further, although in practise a still larger sample of GRB and CCSN hosts may be necessary to place strong constraints. The main bias bias effects on the distributions of *B* and *V* absolute magnitudes are redshift method, and dust obscured hosts. Both emission line redshifts and dust will bias the GRB sample towards brighter hosts, while dust in CCSN hosts will give us a fainter sample – although a quantitative estimation of how large these effects are is difficult, they are acting in opposite directions, suggesting a fainter true GRB host population and a brighter true CCSN population.

Since the absolute magnitude distributions of the two populations show only modest differences, it is unsurprising that the global distributions of other parameters which depend directly on the magnitude in a given band (principally mass and SFR) are also similar.

Further, since GRB hosts are on average bluer and of lower mass (even though the difference between each distribution are not significant in their own right) the distinction in the SSFR is much stronger (this is also in part since the order of individual galaxies is obviously not identical in the mass and SFR cumulative distributions). In Fig. 7, we plot the SSFRs versus the stellar masses in the host galaxies. The majority of the GRB hosts are located in the low mass, high SSFR area, only a small fraction of the hosts demonstrate high mass and low SSFR. The *KS* test on the SSFR accepts, with a good statistical significance that GRB hosts typically have higher SSFRs than CCSN hosts.

While the estimated stellar masses and SFRs are compatible with a common distribution, we note that galaxy and stellar population age can have the effect on our measurements to overestimate the mass, and underestimate the SFR for young starbursts as discussed previously, while also dust obscuration will narrow the mass distributions of the samples. Hence, it is *possible* that the mass and SFR distributions are more diverse than a direct interpretation our results would indicate. This suggestion is further supported by simple morphological analysis of the host galaxy samples, which show striking differences. In the sample of CCSN hosts the spiral fraction is approximately $27/58 \sim 0.45$ with a Poisson counting error $\sim$5. If the GRB host sample has identical spiral fraction, the expected number of spirals is $\sim 15 \pm 4$, whereas only two can be recognized as spirals in the GRB host sample (GRBs 990705 and 020819).[6] The Poisson probability of two or less spiral galaxies to be found in a sample with an expected spiral fraction of 0.45 is $\sim 4 \times 10^{-5}$.

Performing a more quantitative analysis on the physical sizes of the hosts reveals that GRB hosts are also significantly smaller than CCSN hosts. A comparison of the 80 per cent light radii using the KS test results in $P_{\rm KS} = 0.003$ that the sizes are drawn from the same parent distribution. In Fig. 6, we plotted r_{80} versus M_V. Visual inspection confirms that the GRB host population is smaller than the CCSN host population, which is accepted by the KS test, and is in excellent agreement with with the morphological distribution – small irregulars versus large grand design spirals.

As an alternative to estimating mass from the *K*-band luminosity, we note that there is also a strong trend in the size-stellar mass relation (e.g. Shankar & Bernardi 2009). Since the luminosity based mass estimates suggest consistent distributions for the CCSN and GRB samples, but the size distributions are inconsistent, *both* of these relations cannot be correct. Due to the uncertainties in stellar population ages, and their contributions to the *K*-band luminosities, we suggest that size is a more stable proxy for mass when comparing samples of potentially different ages. Inserting the size distributions into any size-to-mass relation would hence yield a significantly lower mass distribution than estimated by the *K*-band luminosity and result in a KS probability for the mass identical to that of r_{80}. However, if this argument is wrong, and the *K*-band mass estimates are indeed correct, this would suggest that the host masses are more similar than previously though, and implications on global environments and metallicities would put constraints on the collapsar model.

The low probability of the size and morphological distributions being compatible is obviously in conflict with the apparently similar mass (*K*-band luminosity) distributions discussed above, and does suggest markedly different large scale environments. Assuming that GRB hosts have *similar mass* distributions but *smaller size* distribution than the CCSN host sample, we look at size – metallicity relations at constant mass. A positive correlation between size and metallicity is found by Hoopes et al. (2007) for UV selected and galaxies and by Ellison et al. (2008b) for galaxies in close pairs. On the opposite side, Ellison et al. (2008a) indicate that the *M–Z* relation in $\sim$44 000 SDSS galaxies is offset to higher metallicities for galaxies with decreasing size.

The ambiguity of these results can be interpreted in two ways. If the estimates mirror the true distributions, then we can deduce that GRB hosts, and progenitor stars, have similar mass and metallicity distributions, but have significantly higher stellar densities. Alternatively, if the estimated mass distributions are dominated by galaxy-evolutionary or dust obscuration bias effects, then the GRB hosting population could be significantly less massive than it appears from the *K*-band estimates. Instead, if the mass-to-light ratio is violated, galaxy size will be a more stable indicator if galaxy mass. This notion is supported by strong trends in the size-stellar mass relation (e.g. Shankar & Bernardi 2009), which also notes the age dependency of this relation establishes smaller sizer for old galaxies at a given mass – hence we can be certain that galaxy evolution is not a major concern for galactic sizes.

10 SUMMARY

We have used multiwavelength photometry to investigate the physical properties of long GRBs and CCSN hosting galaxies at low to intermediate redshifts. We fit SEDs and estimate rest-frame absolute magnitudes, stellar masses and SFRs. From the stellar masses we have also attempted to estimate host metallicities. Galaxy sizes and morphologies are studied. Our results show that within our sample the derived masses and absolute magnitudes are not significantly different between the two populations, although the majority of likely selection effects act to shrink any intrinsic separation within the two samples. Indeed, while not statistically significant in terms of a *KS* test, the cut-off in the luminosity function of GRB hosts about 1 mag fainter than the CCSN hosts, is suggestive of a metallicity cut-off. Further, the physical sizes and morphologies within the two samples are different with high statistical significance, and this lends further support to models in which GRBs form only in certain environmental conditions, most likely related to low mass and metallicity.

Finally, the locations of the bursts and CCSNe on their hosts, measured both in absolute terms, and relative to their cumulative light distributions shows GRBs to be highly concentrated on their host light, and to be occurring in regions of high absolute surface brightness.

To summarize our interpretation in terms of current models for GRB production we suggest the following.

(i) GRB hosts are consistently smaller than CCSN hosts.

(ii) The high surface brightness, surface SFRs and relative locations on hosts suggest that GRBs are originating in a younger, and more massive stellar population.

(iii) This and other lines of evidence suggest that the dominant stellar populations in GRB hosts are very young. This may introduce systematic errors which overestimate stellar mass and underestimate SFRs.

ACKNOWLEDGMENTS

KMS thank the University of Warwick for doctoral studentship, AJL and NRT thank STFC for postdoctoral and senior fellowship

[6]This count ignores the unusual GRB 980425, but its inclusion only slightly affects the results.

awards. This research has made use of the GHostS data base (www.grbhosts.org), which is partly funded by *Spitzer*/NASA grant RSA Agreement No. 1287913. Based on observations made with the NASA/ESA *Hubble Space Telescope*, obtained from the data archive at the Space Telescope Science Institute. STScI is operated by the Association of Universities for Research in Astronomy, Inc. under NASA contract NAS 5-26555. The observations are associated with programme numbers 11513, 10189, 9352, 9074, 9405, 10551, 10135, 9180 and 8688. Finally, we also thank the anonymous referee for a constructive report.

REFERENCES

Berger E. et al., 2002, ApJ, 581, 981
Bernardi M. et al., 2003, AJ, 125, 1849
Berta S., Fritz J., Franceschini A., Bressan A., Lonsdale C., 2004, A&A, 418, 913
Bertin E., Arnouts S., 1996, A&AS, 117, 393
Bloom J. S. et al., 2009, ApJ, 691, 723
Bruzual A. G., Charlot S., 1993, ApJ, 405, 538
Calzetti D., Armus L., Bohlin R. C., Kinney A. L., Koornneef J., Storchi-Bergmann T., 2000, ApJ, 533, 682
Castro Cerón J. M., Michałowski M. J., Hjorth J., Watson D., Fynbo J. P. U., Gorosabel J., 2006, ApJ, 653, L85
Chary R., Dickinson M. E., Teplitz H. I., Pope A., Ravindranath S., 2005, ApJ, 635, 1022
Chen H.-W., Prochaska J. X., Bloom J. S., Thompson I. B., 2005, ApJ, 634, L25
Christensen L., Hjorth J., Gorosabel J., 2004, A&A, 425, 913
Christensen L., Vreeswijk P. M., Sollerman J., Thöne C. C., Le Floc'h E., Wiersema K., 2008, A&A, 490, 45
Coleman G. D., Wu C.-C., Weedman D. W., 1980, ApJS, 43, 393
Cram L., Hopkins A., Mobasher B., Rowan-Robinson M., 1998, ApJ, 507, 155
Dahlen T., Strolger L., Riess A. G., 2008, ApJ, 681, 462
Damjanov I. et al., 2009, ApJ, 695, 101
Ellison S. L., Patton D. R., Simard L., McConnachie A. W., 2008a, ApJ, 672, L107
Ellison S. L., Patton D. R., Simard L., McConnachie A. W., 2008b, AJ, 135, 1877
Fruchter A., Krolik J. H., Rhoads J. E., 2001, ApJ, 563, 597
Fruchter A. S. et al., 2006, Nat, 441, 463 (F06)
Fynbo J. U. et al., 2001, A&A, 369, 373
Fynbo J. P. U. et al., 2006, Nat, 444, 1047
Fynbo J. P. U. et al., 2009, ApJS, 185, 526
Garnett D. R., Shields G. A., Skillman E. D., Sagan S. P., Dufour R. J., 1997, ApJ, 489, 63
Gehrels N. et al., 2006, Nat, 444, 1044
Giavalisco M. et al., 2004, ApJ, 600, L93
Glazebrook K. et al., 2004, Nat, 430, 181
Grazian A. et al., 2006, A&A, 449, 951
Groot P. J. et al., 1998, ApJ, 493, L27
Heger A., Fryer C. L., Woosley S. E., Langer N., Hartmann D. H., 2003, ApJ, 591, 288
Hjorth J. et al., 2003, ApJ, 597, 699
Hoopes C. G. et al., 2007, ApJS, 173, 441
Jakobsson P., Hjorth J., Fynbo J. P. U., Watson D., Pedersen K., Björnsson G., Gorosabel J., 2004, ApJ, 617, L21
Jakobsson P. et al., 2005, MNRAS, 362, 245
Jakobsson P. et al., 2006, A&A, 447, 897
James P. A., Anderson J. P., 2006, A&A, 453, 57
Kelly P. L., Kirshner R. P., Pahre M., 2008, ApJ, 687, 1201
Larson R. B., 1974, MNRAS, 169, 229
Larsson J., Levan A. J., Davies M. B., Fruchter A. S., 2007, MNRAS, 376, 1285
Lazzati D., Covino S., Ghisellini G., 2002, MNRAS, 330, 583
Le Floc'h E., Charmandaris V., Forrest W. J., Mirabel I. F., Armus L., Devost D., 2006, ApJ, 642, 636
Leitherer C., Heckman T. M., 1995, ApJS, 96, 9
Lequeux J., Peimbert M., Rayo J. F., Serrano A., Torres-Peimbert S., 1979, A&A, 80, 155
Levan A. et al., 2006a, ApJ, 647, 471
Levan A. J., Davies M. B., King A. R., 2006b, MNRAS, 372, 1351
Levesque E. M., Kewley L. J., Larson K., Snijders L., 2008, in Hunt L. K., Madden S., Schneider R., eds, Proc. IAU Symp. 255, Modeling the ISM Properties of Metal Poor Galaxies and Gamma-Ray Burst Hosts. Kluwer, Dordrecht, p. 162
Levesque E. M., Berger E., Kewley L. J., Bagley M. M., 2009, preprint (arXiv:0907.4988)
McBreen S. et al., 2008, ApJ, 677, L85
Madau P., della Valle M., Panagia N., 1998, MNRAS, 297, L17
Mannucci F. et al., 2003, A&A, 401, 519
Masetti N. et al., 2000, A&A, 354, 473
Michałowski M. J., Hjorth J., Castro Cerón J. M., Watson D., 2008, ApJ, 672, 817
Modjaz M. et al., 2008, AJ, 135, 1136
Östlin G., Zackrisson E., Sollerman J., Mattila S., Hayes M., 2008, MNRAS, 387, 1227
Pei Y. C., Fall S. M., 1995, ApJ, 454, 69
Perley D. A. et al., 2009, preprint (arXiv:0905.0001)
Podsiadlowski P., Mazzali P. A., Nomoto K., Lazzati D., Cappellaro E., 2004, ApJ, 607, L17
Prieto J. L., Stanek K. Z., Beacom J. F., 2007, preprint (arXiv:0707.0690)
Racusin J. L. et al., 2008, Nat, 455, 183
Raskin C., Scannapieco E., Rhoads J., Della Valle M., 2008, ApJ, 689, 358
Riess A. G. et al., 2004, ApJ, 600, L163
Rol E. et al., 2007, ApJ, 669, 1098
Rolleston W. R. J., Smartt S. J., Dufton P. L., Ryans R. S. I., 2000, A&A, 363, 537
Savaglio S. et al., 2005, ApJ, 635, 260
Savaglio S., Glazebrook K., Le Borgne D., 2009, ApJ, 691, 182
Schlegel D. J., Finkbeiner D. P., Davis M., 1998, ApJ, 500, 525
Shankar F., Bernardi M., 2009, MNRAS, 396, L76
Silva L., Granato G. L., Bressan A., Danese L., 1998, ApJ, 509, 103
Starling R. L. C. et al., 2005, A&A, 442, L21
Strolger L.-G. et al., 2004, ApJ, 613, 200
Tanvir N. R. et al., 2010, preprint (arXiv:0812.1217)
Thöne C. C. et al., 2008, ApJ, 676, 1151
Tremonti C. A. et al., 2004, ApJ, 613, 898
van den Heuvel E. P. J., Yoon S.-C., 2007, Ap&SS, 311, 177
Vanzella E. et al., 2005, A&A, 434, 53
Vanzella E. et al., 2006, A&A, 454, 423
Vanzella E. et al., 2008, A&A, 478, 83
Verma A., Lehnert M. D., Förster Schreiber N. M., Bremer M. N., Douglas L., 2007, MNRAS, 377, 1024
Vreeswijk P. M. et al., 2004, A&A, 419, 927
Wirth G. D. et al., 2004, AJ, 127, 3121
Wolf C., Podsiadlowski P., 2007, MNRAS, 375, 1049
Woosley S. E., 1993, ApJ, 405, 273
Yoon S.-C., Langer N., 2005, A&A, 443, 643

APPENDIX A

Table A1. Photometric catalogue over CCSN host galaxies in the GOODS fields. Errors are 1σ standard errors, limits are 3σ limiting magnitudes estimated from the sky background.

SN name	*B*	*V*	*I*	*Z*	*J*	*H*	*K*
2002fv	28.94 ± 0.53	28.16 ± 0.21	26.78 ± 0.12	26.89 ± 0.17	>27.82	>24.17	>26.96
2002fz	23.23 ± 0.19	22.4 ± 0.07	21.45 ± 0.07	21.11 ± 0.08	>23.78		20.01 ± 0.02
2002hs	24.17 ± 0.17	23.93 ± 0.12	23.51 ± 0.18	23.06 ± 0.17	23.25 ± 0.05	23.02 ± 0.62	22.70 ± 0.05
2002hq	21.93 ± 0.18	21.08 ± 0.06	20.19 ± 0.07	19.90 ± 0.08	19.45 ± 0.02	19.23 ± 0.14	18.85 ± 0.02
2002kb	21.47 ± 0.14	20.64 ± 0.05	20 ± 0.07	19.78 ± 0.08	19.3 ± 0.02	19.18 ± 0.17	18.89 ± 0.03
2002ke		21.45 ± 0.05	20.72 ± 0.07	20.47 ± 0.08			
2002kl	23.32 ± 0.13	22.69 ± 0.06	22.28 ± 0.1	22.18 ± 0.13			
2003ba	21.07 ± 0.04	20.06 ± 0.01	19.63 ± 0.02	19.43 ± 0.03			
2003bb	22.32 ± 0.29	21.62 ± 0.12	20.71 ± 0.13	20.24 ± 0.12			
2003bc	22.6 ± 0.05	21.78 ± 0.02	21.29 ± 0.03	21.14 ± 0.04			
2003dx	24.02 ± 0.04	23.31 ± 0.02	22.78 ± 0.02	22.65 ± 0.03			
2003dz	25.51 ± 0.18	25.28 ± 0.14	24.79 ± 0.19	24.57 ± 0.24			
2003en	25.78 ± 0.06	25.34 ± 0.04	24.53 ± 0.04	24.49 ± 0.04			
2003er	22.65 ± 0.12	21.40 ± 0.03	20.41 ± 0.03	20.05 ± 0.03			
2003et	23.34 ± 0.04	23.09 ± 0.03	22.73 ± 0.04	22.25 ± 0.04			
2003ew	23.55 ± 0.14	22.61 ± 0.05	21.76 ± 0.05	21.45 ± 0.06			
2003N	24.96 ± 0.16	24.7 ± 0.11	24.32 ± 0.17	23.88 ± 0.17			
K0404-005	24.95 ± 0.08	22.88 ± 0.01	21.23 ± 0.01	20.57 ± 0.0			
K0404-003	27.19 ± 0.14	27.13 ± 0.14	26.53 ± 0.16	26.43 ± 0.17			
K0404-006	24.03 ± 0.02	23.45 ± 0.01	23.02 ± 0.02	22.77 ± 0.02			
K0404-008	21.15 ± 0.01	19.84 ± 0.0	19.16 ± 0.0	18.83 ± 0.0			
K0404-010	27.45 ± 0.44	25.26 ± 0.05	23.76 ± 0.03	23.22 ± 0.02			
K0405-001	22.39 ± 0.01	21.66 ± 0.01	21.04 ± 0.01	20.87 ± 0.01			
K0405-002	22.39 ± 0.01	21.62 ± 0.01	21 ± 0.01	20.83 ± 0.01			
K0405-005	26.04 ± 0.11	25.24 ± 0.04	24.37 ± 0.04	24.33 ± 0.05			
K0405-007	24.14 ± 0.03	23.03 ± 0.01	22.21 ± 0.01	21.91 ± 0.01			
K0405-008	27.02 ± 0.23	26.22 ± 0.09	25.59 ± 0.1	24.89 ± 0.06			
HST04Pata		20.13 ± 0.0	19.56 ± 0.0	19.26 ± 0.0			
HST04Cli	26.92 ± 0.16	25.85 ± 0.05	25.42 ± 0.06	25.47 ± 0.08	24.22 ± 0.5		23.28 ± 0.32
HST04Wil	22.65 ± 0.01	21.72 ± 0.01	21.27 ± 0.01	21.08 ± 0.01	20.83 ± 0.1	20.75 ± 0.1	20.61 ± 0.09
HST04Pol	22.22 ± 0.01	21.43 ± 0.0	20.74 ± 0.0	20.5 ± 0.0	20.15 ± 0.07	19.91 ± 0.07	19.62 ± 0.06
HST04Jef	25.7 ± 0.1	25.83 ± 0.1	24.99 ± 0.09	25.04 ± 0.13	>27.14	>23.63	>26.31
HST04Ken	23.05 ± 0.02	22.21 ± 0.01	21.56 ± 0.01	>24.43	20.91 ± 0.1	20.74 ± 0.1	20.45 ± 0.08
HST04Cum	25.17 ± 0.05	25.04 ± 0.04	24.58 ± 0.05	24.50 ± 0.05			
HST04Cay	26.75 ± 0.1	25.74 ± 0.03	25.58 ± 0.06	25.39 ± 0.06			
HST04Bon	23.56 ± 0.03	21.94 ± 0.01	20.67 ± 0.0	20.23 ± 0.0	19.59 ± 0.06	19.18 ± 0.05	18.81 ± 0.04
HST04Sos	23.90 ± 0.03	22.8 ± 0.01	22.05 ± 0.01	21.76 ± 0.01	21.37 ± 0.13	21.22 ± 0.12	20.96 ± 0.11
HST04Fox	24.91 ± 0.04	24.6 ± 0.02	24.01 ± 0.03	>26.36	23.92 ± 0.42	23.73 ± 0.39	23.43 ± 0.34
HST04Con	23.43 ± 0.02	22.95 ± 0.01	22.08 ± 0.01	21.76 ± 0.01			
HST04Hei	21.47 ± 0.14	20.64 ± 0.05	20.00 ± 0.07	19.78 ± 0.08	19.3 ± 0.02	19.18 ± 0.17	18.89 ± 0.03
HST04Riv	26.45 ± 0.13	25.64 ± 0.05	24.80 ± 0.05	>26.18	24.47 ± 0.56	25.18 ± 0.79	24.36 ± 0.53
HST04Geo	24.26 ± 0.03	24.08 ± 0.03	23.36 ± 0.03	23.12 ± 0.02			
HST04Gua	26.11 ± 0.17	24.36 ± 0.04	22.66 ± 0.01	21.66 ± 0.01			
HST04Ida	27.10 ± 0.11	26.29 ± 0.08	26.49 ± 0.21	26.59 ± 0.3			
HST05Kir	24.66 ± 0.04	24.43 ± 0.03	23.98 ± 0.03	24.10 ± 0.05			
HST05Pic	23.60 ± 0.02	23.47 ± 0.02	22.81 ± 0.02	22.65 ± 0.02			
HST05Sev	24.15 ± 0.05	24.18 ± 0.04	23.66 ± 0.04	23.32 ± 0.04			
HST05Sco	25.20 ± 0.06	25.34 ± 0.06	24.58 ± 0.06	24.35 ± 0.06			
HST05Boy	25.45 ± 0.05	25.29 ± 0.04	24.80 ± 0.05	>26.37	24.29 ± 0.51		24.24 ± 0.52
HST05Den	25.30 ± 0.07	24.78 ± 0.04	23.92 ± 0.03	23.53 ± 0.03			
HST05Bra	23.32 ± 0.02	22.28 ± 0.01	21.63 ± 0.01	21.36 ± 0.01			
HST05Str	24.03 ± 0.04	23.84 ± 0.04	23.21 ± 0.03	22.93 ± 0.03			
HST05Ste	24.34 ± 0.23	23.75 ± 0.09	23.32 ± 0.1	23.51 ± 0.1			
HST05Cas	26.33 ± 0.15	25.83 ± 0.08	24.98 ± 0.07	24.89 ± 0.08			
HST05Mob	24.91 ± 0.05	23.93 ± 0.02	22.97 ± 0.02	22.66 ± 0.01			
HST05Ton	23.22 ± 0.02	22.45 ± 0.01	21.45 ± 0.01	21.15 ± 0.01			
HST05Fil	24.94 ± 0.04	24.73 ± 0.03	24.57 ± 0.04	24.38 ± 0.04			

Table A2. Photometric catalogue continued: *Spitzer* IRAC bands.

SN name	3.6 μm	4.5 μm	5.8 μm	8 μm
2002fv	>25.65	24.52 ± 0.14	>23.58	>24.69
2002fz				
2002hs	21.78 ± 0.01	21.79 ± 0.01	22.37 ± 0.06	22.53 ± 0.06
2002hq	18.89 ± 0.01		19.39 ± 0.03	
2002kb	19.28 ± 0.01	19.95 ± 0.0	19.8 ± 0.13	19.74 ± 0.01
2002ke	19.97 ± 0.01		20.47 ± 0.2	
2002kl	22.4 ± 0.03		23.17 ± 0.21	
2003ba		19.45 ± 0.01		18.55 ± 0.01
2003bb		18.97 ± 0.01		19.43 ± 0.03
2003bc				
2003dx		22.44 ± 0.02		22.46 ± 0.08
2003dz		23.35 ± 0.04		23.66 ± 0.2
2003ea	22.4 ± 0.07	22.78 ± 0.07	23.06 ± 0.38	>23.25
2003en	24.58 ± 0.24	25.33 ± 0.25	>22.93	>25.44
2003er		19.55 ± 0.0		20.08 ± 0.03
2003et		20.89 ± 0.01		21.19 ± 0.02
2003ew		21.16 ± 0.01		21.34 ± 0.05
2003N	21.86 ± 0.02	21.86 ± 0.01	22.04 ± 0.07	22.2 ± 0.1
K0404-005	18.99 ± 0.0	19.52 ± 0.0	19.67 ± 0.01	20.13 ± 0.04
K0404-003		24.71 ± 0.16		23.44 ± 0.26
K0404-006	21.03 ± 0.01		20.79 ± 0.02	
K0404-008	18.02 ± 0.0		18.33 ± 0.01	
K0404-010	21.71 ± 0.02	23.52 ± 0.03	22.76 ± 0.19	22.9 ± 0.12
K0405-001		20.99 ± 0.01		21.19 ± 0.05
K0405-002		20.98 ± 0.01		20.97 ± 0.05
K0405-005	24.03 ± 0.07	24.29 ± 0.1	>23.97	>24.23
K0405-007				
K0405-008	23.1 ± 0.06		23.15 ± 0.2	
HST04Pata	18.86 ± 0.0	19.26 ± 0.0	19.25 ± 0.03	17.97 ± 0.02
HST04Cli	22.88 ± 0.13		22.47 ± 0.11	
HST04Wil	20.91 ± 0.03		21.43 ± 0.07	
HST04Pol	19.83 ± 0.01	20.2 ± 0.0	20.19 ± 0.04	20.28 ± 0.05
HST04Jef				
HST04Ken				
HST04Cum	23.21 ± 0.05	23.5 ± 0.05	23.69 ± 0.23	>24.06
HST04Cay	23.65 ± 0.05	23.83 ± 0.08	23.11 ± 0.27	23.79 ± 0.32
HST04Bon	18.97 ± 0.0	19.32 ± 0.0	19.34 ± 0.01	19.51 ± 0.01
HST04Sos	21.21 ± 0.02	21.54 ± 0.01	21.76 ± 0.08	21.82 ± 0.06
HST04Fox		24.23 ± 0.09		>24.54
HST04Con	20.77 ± 0.0	21.25 ± 0.01	21.2 ± 0.05	21.88 ± 0.07
HST04Hei	19.28 ± 0.01	19.95 ± 0.0	19.8 ± 0.13	19.74 ± 0.01
HST04Riv	23.89 ± 0.06		23.97 ± 0.44	
HST04Geo		23.13 ± 0.02		23.72 ± 0.23
HST04Gua	18.74 ± 0.03		19.18 ± 0.04	
HST04Ida		24.32 ± 0.16		>24.21
HST05Kir				
HST05Pic	22.42 ± 0.03		22.69 ± 0.26	
HST05Sev	23.51 ± 0.08		23.47 ± 0.38	
HST05Sco	22.06 ± 0.03		22.7 ± 0.17	
HST05Boy		24.8 ± 0.26		>24.47
HST05Den	22.65 ± 0.03	22.75 ± 0.02	23.05 ± 0.12	23.05 ± 0.17
HST05Bra	20.82 ± 0.0	21.04 ± 0.01	21.11 ± 0.03	20.93 ± 0.04
HST05Str	21.99 ± 0.07	22.4 ± 0.06	>22.1	22.55 ± 0.13
HST05Cas		>26.07		>24.67
HST05Mob	21.3 ± 0.03	21.87 ± 0.01	21.85 ± 0.1	22.37 ± 0.09
HST05Ton	19.79 ± 0.0	20.28 ± 0.0	20.23 ± 0.03	20.51 ± 0.02
HST05Fil	23.32 ± 0.06		>24.25	
HST05Ste	23.54 ± 0.09		>23.81	

Table A3. GRB host photometry in the *Spitzer* IRAC bands. Limits are 3σ background estimates, errors are 1σ.

GRB	3.6 μm	4.5 μm	5.8 μm	8 μm
970228	22.02 ± 0.2		>20.02	
990712		21.98 ± 0.4		>19.42
991208		>22.21		>20.57
000210		21.76 ± 0.23		20.48 ± 0.25
000911		>22.12		>18.41
010921	21.74 ± 0.43		>20.15	
020405	20.81 ± 0.15		>19.82	
020819	18.96 ± 0.02		19.27 ± 0.22	
021211		21.24 ± 0.24		>18.57
030329	>22.59		>18.96	
031203	18.19 ± 0.03		17.6 ± 0.06	
040924	>21.92		>19.81	
041006	21.43 ± 0.19		>20.0	

This paper has been typeset from a TEX/LATEX file prepared by the author.